

Multifaceted actions of Zeb2 in postnatal neurogenesis from the ventricular-subventricular zone to the olfactory bulb

Astrid Deryckere^{1,\$}, Elke Stappers^{2,3,\$}, Ruben Dries^{2,3,#}, Elise Peyre⁴, Veronique van den Berghe^{2,5}, Andrea Conidi³, F. Isabella Zampeta³, Annick Francis², Marjolein Bresseleers², Agata Stryjewska^{2,#}, Ria Vanlaer¹, Elke Maas⁶, Ihor V. Smal^{3,7}, Wilfred F. J. van IJcken^{3,8}, Frank G. Grosveld³, Laurent Nguyen⁴, Danny Huylebroeck^{2,3,*}, Eve Seuntjens^{1,2,*&}

¹ Laboratory of Developmental Neurobiology, Department of Biology, KU Leuven, Belgium; ² Laboratory of Molecular Biology (Celgen), Department of Development and Regeneration, KU Leuven, Belgium; ³ Department of Cell Biology, Erasmus University Medical Center, Rotterdam, The Netherlands; ⁴ GIGA-Stem Cells and GIGA-Neurosciences, Liège University, Belgium; ⁵ Centre for Developmental Neurobiology, Institute of Psychiatry, Psychology and Neuroscience, and MRC Centre for Neurodevelopmental Disorders, King's College London, UK; ⁶ Department of Cardiovascular Sciences, Center for Molecular and Vascular Biology, KU Leuven, Belgium; ⁷ Department of Molecular Genetics, Erasmus University Medical Center, Rotterdam, The Netherlands; ⁸ Center for Biomics-Genomics, Erasmus University Medical Center, Rotterdam, The Netherlands.

[#] Present addresses: (RD) Department of Medicine, Harvard Medical School, and Department of Medical Oncology, Dana-Farber Cancer Institute, Boston, U.S.A.; (AS) Neural Development, Plasticity and Repair, Wolfson Institute for Biomedical Research, University College London, U.K.; (EM) Laboratory of Virology and Chemotherapy (Rega Institute), KU Leuven, Belgium

^{\$} Shared first and * shared senior authors

[&] Corresponding author:

Eve Seuntjens, Dept. Biology, KU Leuven, Naamsestraat 61, 3000 Leuven, Belgium

Tel:+32-16-373135 E-mail: eve.seuntjens@kuleuven.be

Key words: postnatal neurogenesis, NuRD, olfactory bulb, Smad, ventricular-subventricular zone, Zeb2

Summary statement

The transcription factor Zeb2 uses distinct molecular subdomains to regulate olfactory bulb interneuron generation and maturation from the young postnatal ventricular-subventricular zone in mice.

ABSTRACT

The transcription factor Zeb2 controls fate specification and subsequent differentiation and maturation of multiple cell types in various embryonic tissues. It binds many protein partners, including activated Smad proteins and the NuRD co-repressor complex. How Zeb2 subdomains support cell differentiation in various contexts has remained elusive. Here, we have studied the role of Zeb2 and its domains in neurogenesis and neural differentiation in the young postnatal ventricular-subventricular zone (V-SVZ), where neural stem cells generate olfactory bulb-destined interneurons. Conditional *Zeb2* knockouts and separate acute loss- and gain-of-function approaches indicated that Zeb2 is essential to control apoptosis and neuronal differentiation of V-SVZ progenitors before and after birth, and identified *Sox6* as Zeb2-dependent and potential downstream target gene. *Zeb2* genetic inactivation impaired the differentiation potential of the V-SVZ niche in a cell-autonomous fashion. We also provide evidence that its normal function in the V-SVZ involves non-autonomous mechanisms as well. Additionally, we could demonstrate distinct roles for Zeb2 protein-binding domains, suggesting that Zeb2 partners co-determine neuronal output from the mouse V-SVZ in both quantitative and qualitative manners in early postnatal life.

INTRODUCTION

Neurogenesis in the central nervous system starts during embryonic development and continues after birth in two discrete regions of the mammalian brain: the subgranular zone (SGZ) of the hippocampal dentate gyrus and the ventricular-subventricular zone (V-SVZ) lining the lateral ventricle walls. In rodents, newly formed SGZ neurons integrate locally, whereas V-SVZ neuroblasts migrate over long distance before integrating and maturing in the olfactory bulb (OB) (Altman, 2011; Lim and Alvarez-Buylla, 2014; Urbán and Guillemot, 2014).

The postnatal neurogenic zones have an embryonic origin. In the case of the V-SVZ, a fraction of forebrain radial glial cells (RGCs) in the lateral ganglionic eminences (LGEs) and pallium becomes quiescent (Young *et al.*, 2007; Fuentealba *et al.*, 2015). These progenitor cells are reactivated early after birth and differentiate into either supportive, niche-regulatory ependymal cells or radial glial-like neural stem cells (NSCs or B1 cells) of the V-SVZ (Mirzadeh *et al.*, 2008; Fuentealba *et al.*, 2015). These B1 cells proliferate slowly and generate transit-amplifying cells (C cells), which in turn give rise to immature migratory neuroblasts (A cells). Neuroblasts migrate via the rostral migratory stream (RMS) towards the OB where they disperse radially, and eventually mature into network integrated periglomerular or granular interneurons (Doetsch and Alvarez-Buylla, 1996; Doetsch, García-Verdugo and Alvarez-Buylla, 1997; Alvarez-Buylla and García-Verdugo, 2002; Bjornsson *et al.*, 2015; Lim and Alvarez-Buylla, 2016). In addition to these GABAergic interneurons, the OB contains glutamatergic tufted and mitral cells as well as juxtaglomerular interneurons (Blanchart, De Carlos and López-Mascaraque, 2006; Brill *et al.*, 2010; Díaz-Guerra *et al.*, 2013).

Interneuron diversity in the OB is achieved through a combination of temporal and regional controls, for proliferating NSCs generate distinct populations of OB interneuron at different time points (Lemasson, Saghatelian and Lledo, 2005; Batista-Brito, Close, *et al.*, 2008). Neurons born in the first postnatal week are more prone to become superficial granule cells compared to cells born later (Lemasson, Saghatelian and Lledo, 2005). Furthermore, extrinsic and intrinsic factors, epigenetic and transcriptional controls, and apoptosis influence OB interneuron production, fate specification and maturation (reviewed in Díaz-Guerra *et al.*, 2013; Lim and Alvarez-Buylla, 2016).

Zeb2 (Sip1, Zfhx1b) is a DNA-binding transcription factor that binds E-box-like sequences in gene regulatory regions (Remacle *et al.*, 1999; Verschueren *et al.*, 1999). In humans, *de novo* mutation of one *ZEB2* allele causes Mowat-Wilson Syndrome (MOWS; OMIM#235730) (Mowat *et al.*, 1998; Cacheux *et al.*, 2001; Wakamatsu *et al.*, 2001), while mutations in *ZEB1*, the second member of this family, cause corneal dystrophy in the eye (Chung *et al.*, 2014). MOWS is a severe developmental disorder affecting both the neural crest and neural lineages. It is characterized by typical impediment of craniofacial development, severe intellectual disability in most patients, and in many cases epilepsy

and Hirschsprung disease (Zweier *et al.*, 2002, 2005; Garavelli and Mainardi, 2007; Ivanovski *et al.*, 2018).

Murine Zeb2 is 1,215 amino acids long and structurally similar to Zeb1 (δ EF1, Zfhx1a) (Funahashi *et al.*, 1991). Both have two separated clusters of zinc fingers (NZF and CZF) wherein the two last fingers each bind predominantly to 5'-CACCT(G) on target DNA (Sekido *et al.*, 1994; Remacle *et al.*, 1999). Zeb2 NZF and CZF domains are separated by a Smad-binding domain (SBD) and, similar to Zeb1, a non-DNA-binding homeodomain-like domain (HD) and a domain serving interaction with CtBP1/2 co-repressors (CID). Both Zeb proteins also contain a short motif (designated as NIM) located close to the N-terminus for binding to the nucleosome remodeling and deacetylation complex (NuRD) (Verschueren *et al.*, 1999; Van Grunsen *et al.*, 2001; Verstappen *et al.*, 2008; Conidi *et al.*, 2011, 2013). In MOWS patients, about 300 *ZEB2* genetic mutations have been mapped so far. Most mutations lead to a C-terminal truncated unstable protein (Zweier *et al.*, 2005; Garavelli *et al.*, 2009; Ivanovski *et al.*, 2018). However, some missense or in-frame deletion mutations in *ZEB2* protein-encoding exons have been described, which usually lead to a milder form of MOWS (Yoneda *et al.*, 2002; Gregory-Evans *et al.*, 2004; Zweier *et al.*, 2005, 2006; Heinritz *et al.*, 2006). For example, mutations disrupting a splice site affecting the interaction of Zeb2 with NuRD cause a mild form of MOWS, associated with fewer psychomotor developmental difficulties or less striking facial gestalt, as well as absence of other anomalies such as agenesis of the corpus callosum and heart defects (Yoneda *et al.*, 2002; Zweier *et al.*, 2006; Verstappen *et al.*, 2008).

Conditional, cell-type specific *Zeb2* knockouts (cKOs) in the mouse have helped to understand MOWS-related neurodevelopmental defects (reviewed in Conidi *et al.*, 2011; Hegarty, Sullivan and O'Keeffe, 2015). During cortical development, Zeb2 directs proper timing of neurogenesis and gliogenesis, and is essential for guided migration of ventral forebrain-born cortical interneurons (Seuntjens *et al.*, 2009; McKinsey *et al.*, 2013; van den Berghe *et al.*, 2013). Correct cortical interneuron migration requires intact zinc finger (ZnF) and SBD domains in Zeb2 (Conidi *et al.*, 2013).

While it has been shown that reduced levels of micro-RNAs of the miR-200 cluster induced *Zeb2* expression and premature differentiation of OB interneurons (Beclin *et al.*, 2016), the precise role of Zeb2 (and its domains) in postnatal neurogenesis and OB interneuron maturation remains unknown. Here, using a combination of Cre-dependent *Zeb2* cKO, and acute loss- versus gain-of-function approaches, we show that Zeb2 controls the numerical output from the V-SVZ as well as differentiation of OB interneurons. Intriguingly, non-Cre-targeted cells also display phenotypes in both processes, indicating that Zeb2 acts partly in a non-cell-autonomous fashion. RNA-sequencing (RNA-seq), ChIP and functional analysis identified *Sox6* as a target of Zeb2. Rescue experiments using domain-mutants of Zeb2 in cKO settings differentially affected OB interneuron development. Hence,

Zeb2 integrates diverse signals and teams up with different partner proteins in the young postnatal V-SVZ niche in order to steer OB interneuron development.

RESULTS

Knockout of *Zeb2* in the embryonic LGE severely disrupts development of the OB

At the time when B cells are set aside in the embryonic brain, Zeb2 mRNA/protein is present in the ventral telencephalon (van den Berghe *et al.*, 2013), including the LGE, which is the major source of B cells for the postnatal V-SVZ (Kriegstein and Alvarez-Buylla, 2009) (Fig. S1A). Zeb2 protein persists in the embryonic and early-postnatal (P)5 and P18 V-SVZ (Fig. S1B-D). In E16.5 and postnatal OBs, Zeb2 was detected throughout the granule cell layers (GCLs) and periglomerular layer (PGL) (Fig. S1E-H), but not in the mitral and external tufted cells, supported by absence of Zeb2 and Reelin co-staining in the P5 OB (Fig. S1I,I') (Hack *et al.*, 2002; Okuyama-Yamamoto *et al.*, 2005).

Zeb2 levels were high in the V-SVZ as well as in OB interneurons, but lower in the migrating neuroblasts in the RMS (Fig. 1A,B). In the niche, Zeb2 was nearly absent from GFAP+ B cells and appeared in EGFR+ C cells and doublecortin+ (Dcx+) A cells (Fig. 1C-E). These expression patterns demonstrate an upregulation of Zeb2 upon maturation and suggest a dual role of Zeb2 in OB interneuron generation and differentiation.

We used Gsh2-Cre mice to inactivate *Zeb2* in the LGE RGCs and their progeny, targeting a large proportion (~70%) of postnatal V-SVZ cells (Stenman, Toresson and Campbell, 2003; Kessaris *et al.*, 2006; Young *et al.*, 2007; van den Berghe *et al.*, 2013). The *Zeb2*-floxed mouse line was first crossed with Cre-dependent GFP-reporter mice (RCE mice) to trace *Zeb2*-KO cells. We confirmed *Zeb2* removal from the LGE at E14.5 in *Zeb2*cKO|Gsh2 mice (Fig. 1F,F'; for strain designations, see Materials and Methods), in the V-SVZ at P2 using RNA-seq on FAC-sorted cells (Fig. S2A) and in tissue sections at P5 (Fig. S3A,B). We also ruled out the possibility of inefficient recombination to produce GFP in the *Zeb2*cKO|Gsh2 V-SVZ, because this could lead to an overestimation of non-cell-autonomous actions of *Zeb2* (Fig. S3C). LGE-specific *Zeb2* removal had major impact on OB development. Less *Zeb2*-KO interneurons were found in the OB, where they failed to distribute over the whole OB and instead clustered in the deep primitive GCLs and later on also around the intermediate plexiform layer (IPL) and mitral cell layer (MCL) (Fig. 1G,H), disturbing the development of the mitral cell layer (Fig. S4). At P17-P18, the mean area of cross-section of *Zeb2*cKO|Gsh2 OBs was 70% smaller, and the OB morphology was more rounded when compared to controls (Fig. 1I-I').

Zeb2 regulates neurogenic output to the OB in the young postnatal V-SVZ

The observed deterioration of the OBs was indicative of a prominent role of Zeb2 in postnatal neurogenesis. Hence, we conducted further analyses of the OBs at P5, when they display a very pronounced phenotype. To assess whether the reduction of OB size in Zeb2cKO|Gsh2 brains was due to decreased numbers of neuroblasts arriving in the OB, we quantified the number of Dcx+ neuroblasts using Dcx mean fluorescence intensity measurements and found a significant decrease in Zeb2cKO|Gsh2 OBs compared to controls (Fig. 1J). Furthermore, the ratio of Dcx+/GFP+ neuroblasts in Zeb2cKO|Gsh2 OBs was 25% smaller compared to controls (Fig. 1K), suggesting that less neuroblasts arrived in the OB.

This reduction in neuroblast numbers in the KOs could arise from the misrouting of interneurons before their entrance in the OB or from their decreased production and/or survival in the V-SVZ. We tested this by *in vivo* electroporation of a TdTomato-encoding vector into the Zeb2cKO|Gsh2 and control V-SVZ at P2. Quantification of TdTomato+ cells in the OB at P9 ensured expression of the construct in the V-SVZ and enabled the tracing of cells derived from the young postnatal niche to the OB (Fig. 2A). Doing so, we found a drastic reduction in number of TdTomato+ cells that had arrived in the Zeb2cKO|Gsh2 OB (Fig. 2B-D). Furthermore, we could not find accumulations of TdTomato+ cells in the V-SVZ or RMS at P9 in Zeb2cKO|Gsh2 mice. In addition, no electroporated cells were found in other regions of the telencephalon, suggesting that the migratory route of these neuroblasts was not impaired. Remarkably, Zeb2-depleted cells within the OB looked morphologically aberrant: whereas control cells were bipolar with a leading process that oriented radially away from the RMS, Zeb2-depleted cells had a stunted shape and appeared disorganized (Fig. 2B'-C'). In particular, we measured the length of the leading process in Zeb2-KO interneurons in the GCL and found that it was 44% shorter compared to controls (Fig. 2E). In the Zeb2-cKO OBs, the number of cells without neurite extension also increased by 30%, while these with one neurite or one branched neurite decreased with 20% and 13%, respectively (Fig. 2F). This suggests that Zeb2 is important for the differentiation and maturation of OB interneurons.

To disentangle the embryonic from postnatal neurogenic actions of Zeb2, we acutely inactivated Zeb2 (by electroporation of a CAGGS-driven Cre-vector) in *Zeb2^{fliko}* and control brains. Notably, in this setup, Zeb2 is depleted from a cohort of cells in the young postnatal V-SVZ that had developed normally, and cells become traceable via Cre-controlled GFP production. We found a similar drastic drop of Zeb2-KO neuron numbers in the OB (Fig. 2G-I), comparable to the embryonic inactivation, and Zeb2-depleted OB interneurons showed a stunted shape and appeared disorganized as well (Fig. 2G'-H'). To assess whether Zeb2-depleted neuroblasts might have arrived at a later time point *in vivo*, we electroporated Cre-vectors in the V-SVZ at P2 and assessed the number of targeted

cells at P56 (*i.e.* 54 days post electroporation) (Fig. S5A). At this late stage too, significantly less GFP+ cells were found in Zeb2cKO|WT compared to control|WT OBs (Fig. S5B,B'), suggesting that delayed migration cannot explain the phenotype.

Collectively, these results suggest that Zeb2 has an essential, cell-intrinsic stimulatory role in regulating the neurogenic output from the early-postnatal V-SVZ.

Zeb2 controls cell survival in the V-SVZ and olfactory bulb

Since Zeb2 levels increase upon progression from NSC to neuroblast in the V-SVZ, we investigated whether Zeb2 acts primarily in B cells, or rather in C or A cells. Hereto, we crossed *Zeb2;RCE*-floxed mice with a Dlx5/6-Cre line, which targets C and A cells in the ganglionic eminences (Stenman, Toresson and Campbell, 2003; van den Berghe *et al.*, 2013). Notably, perinatal lethality of these mice prevents analysis of the phenotype beyond birth (see also van den Berghe *et al.*, 2013). Nevertheless, at E18.5, when V-SVZ derived interneurons are already detectable in the OB, the phenotype caused by the loss of Zeb2 was indistinguishable from the B cell targeting Gsh2-Cre *Zeb2*-cKO (Fig. S6A-D), suggesting that Zeb2 mainly acts in C cells and their progeny.

Given the pronounced decreased OB output, we next assessed cell proliferation in both Gsh2 and Dlx5/6 models in the V-SVZ at E18.5. We did neither observe differences in the number of phospho-histone H3 positive (PH3+, G2/M phase) cells in the E18.5 V-SVZ in the Gsh2 model (Fig. S7A-D) nor in the Dlx5/6 model (Fig. S7E). The situation was different in the postnatal V-SVZ where in the absence of Zeb2, the number of proliferating (Ki67+) cells was reduced, but solely in cells not targeted by Gsh2-Cre (Fig. S7F-I). In order to address postnatal effects only, we used the acute deletion paradigm and analyzed proliferation in the V-SVZ at P5. Again, we did not observe a difference in number of proliferating (Ki67+) targeted cells (Fig. S7J-L). Taken together, our data suggest that there is no overt cell-autonomous proliferation defect in absence of Zeb2 during postnatal neurogenesis.

Another mechanism that could explain the reduction in OB interneurons in absence of Zeb2 is increased apoptosis. Therefore, we quantified the number of cleaved-caspase-3 (CC3) positive cells in the P5 V-SVZ and OB. We found a threefold increase of CC3+ cells in the Zeb2cKO|Gsh2 V-SVZ and a twofold increase in the OB compared to the control (Fig. 3), indicating that Zeb2 promotes survival of OB interneurons at different developmental phases.

Genetic inactivation of Zeb2 affects the maturation of various OB interneuron cell types

Considering the impact of Zeb2-KO on the morphology of OB interneurons, we next tested whether Zeb2-KO affected all types of OB interneuron or rather specific subpopulations. Periglomerular cells in the OB include three major classes of dopaminergic interneuron: TH+, CB+ and calretinin-positive

(Calb2+) cells (Kosaka *et al.*, 1998). In addition, the soma of parvalbumin-positive (PV+) cells are located in the external plexiform layer (EPL). Oncofetal trophoblast glycoprotein 5T4 is present in a specific subtype of OB granule cells found in the GCL and MCL and regulates dendritic arborisation (Batista-Brito, Close, *et al.*, 2008; Yoshihara *et al.*, 2012; Takahashi *et al.*, 2016). We quantified these Calb2+, CB+, PV+, 5T4+ and TH+ interneurons in OBs at P18. This is close to the age at which most Zeb2cKO|Gsh2 mice die, but when expression of the OB interneuron markers is already well established. We found an overall decrease in each of these subtypes, with the exception of Calb2+ cells in Zeb2cKO|Gsh2 as compared to control (Fig. 4). Intriguingly, we also observed a decrease in Cre-targeted (GFP+) as well as non-targeted (GFP-) cells upon Zeb2-cKO for 5T4, CB and PV subtypes (Fig. 4D-I, M-O). Remarkably, non-targeted PV+ interneurons of Zeb2cKO|Gsh2 mice were improperly confined within the boundaries of the RMS in the OB (1% of PV+ cells in control vs 43% in cKO, $p < 0.01$; Fig. 4M-N). We conclude that Zeb2-cKO affects the differentiation of most, but not all OB interneuron subtypes in both cell- and non-cell-autonomous ways.

Upregulation of *Sox6* in Zeb2-depleted cells is an important cause of defective OB interneuron development

To gain more insight into how Zeb2 normally controls the generation of early-postnatal V-SVZ progenitors, we compared transcriptomes of Zeb2cKO|Gsh2 versus control V-SVZ cells after FACS sorting. The respective samples clustered in two highly different groups (Fig. S2B). Principal component analysis (Fig. S2C) showed that they cluster together according to the first principal component (PC1).

Sox6 stood out in the RNA-seq analysis in the Zeb2cKO|Gsh2 V-SVZ as the most upregulated (4.6-fold) gene encoding a transcription factor. *Sox6* steers cortical interneuron development and diversification and is normally found in postmitotic cells of the embryonic ventral telencephalon (Azim *et al.*, 2009; Batista-Brito *et al.*, 2009). In the Zeb2cKO|Gsh2, we found a significant increase of *Sox6* signal in GFP+ as well as GFP- cells within the entire V-SVZ (Fig. 5A-C). RT-qPCR analyses on independent samples confirmed a 3-fold upregulation of *Sox6* steady-state mRNA in Zeb2-mutant V-SVZ cells (*data not shown*). Interestingly, acute deletion of *Zeb2* by Cre-vector electroporation (Fig. 5D) lead to detectable levels of *Sox6*, suggesting that *Sox6* was either induced or failed to be downregulated when *Zeb2* was removed after birth.

These results indicate that *Sox6* may be a direct *Zeb2* target in neurogenic cells of the postnatal V-SVZ. Using chromatin immunoprecipitation (ChIP) in mouse embryonic stem cells (ESCs) subjected to neural differentiation (Stryjewska *et al.*, 2017), we checked whether *Zeb2* binding is enriched in the promoter-proximal regulatory regions of *Sox6*. In line with our previous results

(Stryjewska *et al.*, 2017), we found that both Zeb2 and Sox6 mRNA levels increased from day (d)4 of differentiation, but Sox6 mRNA remained relatively low compared to Zeb2 mRNA (Fig. 5E). In d6 and d8 cells, we found significant enrichment of Zeb2-binding to its cognate sites in the 4 kb-long region upstream of the *Sox6* transcription start site, suggesting that Zeb2 is a candidate direct repressor of *Sox6* (Fig. S8).

When translated to postnatal neurogenesis, these results suggest that overproduction of Sox6 in the wild-type V-SVZ may lead to decreased OB interneuron production, thereby recapitulating the *Zeb2*-cKO phenotype. To test this, we electroporated a (TdTomato and) Sox6-expression vector in the V-SVZ at P2, and quantified the TdTomato+ cells in the OBs at P9 (Fig. 5F). A strong reduction of TdTomato+ cells was found compared to controls (Fig. 5G-I). Of note, we also found similarly aberrant and stunted cellular morphology, comparable to the OB interneurons of *Zeb2*-cKO mice (Fig. 5G'H'). Taken together, these results suggest that Sox6 likely acts downstream of Zeb2.

Different known Zeb2 protein-interacting domains support distinct functions in OB interneuron generation and maturation

To investigate the functions of various known Zeb2 domains in OB interneuron development, we carried out cDNA-based rescue experiments by electroporation (Fig. 6A). For this, we first used a full-length Zeb2 (*Zeb2*^{WT}, Fig. 6B) expression vector in the *Zeb2*cKO|*Gsh2* V-SVZ at P2 (Fig. 6i). As negative control, we used a NZF/CZF double zinc-finger mutant of Zeb2 (*Zeb2*^{ZnF}), which is incapable of binding to DNA (Remacle *et al.*, 1999) (Fig. 6ii). This *Zeb2*^{ZnF} mutant was neither able to rescue defective OB interneuron output, nor interneuron morphology. In contrast, *Zeb2*^{WT} resulted in a 78% increase in neurons, which now again reached the OB when compared to *Zeb2*^{ZnF} (Fig. 6i,ii; quantification in E). Furthermore, most interneurons in this rescue presented with a longer, radially-pointing process, away from the RMS, with several of such cells showing branched processes (Fig. 6F,G).

In *Zeb2*^{SBD}, 4 critical amino acids needed for Smad-binding are substituted, making this mutant protein incapable of binding to activated Smads (Conidi *et al.*, 2013). Electroporation of *Zeb2*^{SBD} resulted in a significantly higher output to the OB (115% increase) and rescued the bipolar morphology, process length and branching of the cells (Fig. 6iv; quantification in E-G). Interestingly, *Zeb2*^{NIM} (a mutant that no longer binds to NuRD (Verstappen *et al.*, 2008; Wu *et al.*, 2016)), did not rescue OB interneuron numbers, but enhanced the formation of cellular processes, and rescued their length and branching capacity, albeit to a lesser extent than *Zeb2*^{SBD} (Fig. 6iii; quantification in E-G). Overproduction of *Zeb2*^{ZnF}, *Zeb2*^{WT} and *Zeb2*^{NIM} in control|*Gsh2* mice resulted in similar cell output to the OB, whereas *Zeb2*^{SBD} caused a 35% increase in number of neurons that arrived at the OB compared to *Zeb2*^{ZnF} (Fig. 6iv, quantification in E).

Taken together, these results show that in the early-postnatal V-SVZ, Zeb2 is essential for the production of sufficient numbers of OB interneurons and for the acquisition of their proper morphology. Furthermore, our experiments indicate that interaction of Zeb2 with receptor-activated Smads normally negatively regulates interneuron output, while interaction with NuRD is necessary for cell maturation, but has no impact on cell number.

DISCUSSION

Zeb2 is implicated in many developmental processes, including exit from epiblast stem cell (-like) pluripotency in ESC cultures (Stryjewska *et al.*, 2017) and in the development of CNS and PNS (for recent reviews, see Hegarty, Sullivan and O’Keeffe, 2015; Epifanova *et al.*, 2019). Here, we show that Zeb2 determines the numeric output from the V-SVZ niche and is needed for normal distribution and maturation of postnatally generated OB interneurons. Furthermore, Zeb2 binds to the *Sox6* promoter and is needed for proper *Sox6* expression control, thereby promoting differentiation of V-SVZ derived cells. In addition, Zeb2 removal also impacts on proliferation and differentiation of non-targeted resident cells. Our results further indicate for the first time that Zeb2 utilizes particular functional domains to perform distinct functions in OB interneuron development, as addressed via cDNA-based rescue experiments in the *Zeb2*-cKO V-SVZ.

Zeb2 as promoter of cell survival, fate specification, and cell differentiation and maturation

In the V-SVZ niche and its progeny, Zeb2 mRNA/protein is present at different temporal levels, being high in V-SVZ C and A cells, decreasing in migrating RMS neuroblasts and becoming more prominent again in cells that progress through differentiation in olfactory periglomerular and granular interneurons. The increased expression upon differentiation in the OB is similar to the one described for other tissues and cells, such as the embryonic cerebral cortex, where Zeb2 is exclusively present in postmitotic cells (Seuntjens *et al.*, 2009), the embryonic ventral telencephalon where it becomes prominent in migrating interneurons (Batista-Brito, MacHold, *et al.*, 2008; McKinsey *et al.*, 2013; van den Berghe *et al.*, 2013), as well as in immune cell maturation (Omilusik *et al.*, 2015; van Helden *et al.*, 2015; Scott *et al.*, 2016), and in human and mouse neural-induced ESCs (Chng *et al.*, 2010; Stryjewska *et al.*, 2017). Here, the pattern suggests Zeb2 plays a role in the V-SVZ niche itself, in particular in the C cells and the neuroblasts, as well as in OB interneurons.

These results, together with the aberrant morphology and reduced numbers of Zeb2-deficient OB interneurons, possibly reflect maturation defects. Similarly, its absence in GABAergic interneurons

leads to deregulation of genes involved in e.g. synaptogenesis and synaptic plasticity (van den Berghe *et al.*, 2013) and Zeb2s' absence also affects midbrain dopaminergic neuron differentiation (Hegarty *et al.*, 2017). Another striking phenotype of Zeb2cKO|Gsh2 mice observed in our study was the failure to populate the OB with neuroblasts in early postnatal life and the reduced output of migrating Dcx+ neuroblasts. We propose that this shortage of OB interneurons in the *Zeb2*-cKO underlies the aberrant OB morphology. Similar disorganization of OB interneurons was observed in *Dlx5/6*-driven *Sp8* and *Sp9*-cKO mice (Waclaw *et al.*, 2006; Li *et al.*, 2018). In *Sp8*-cKO animals however, apoptosis in the V-SVZ, and neuroblast migration and molecular specification defects were exclusively due to defective cell-autonomous actions of *Sp8* (Li *et al.*, 2018).

Functionally integrated, mature interneurons in the GCL of the OB display extensively branched dendritic arbors, and those in the glomerular layer usually have two branched processes (Price and Powell, 1970; Merkle *et al.*, 2014; Figueres-Oñate and López-Mascaraque, 2016). Although our electroporated cells were one week old at most (and hence not fully mature), the processes of the interneurons lacking Zeb2 were absent or shorter, and 73% less-branched compared to controls. A cell-autonomous role for Zeb2 operates in axon length of hippocampal and neocortical cells *in vitro*, as well as in axon branching in the cortex where neurons lacking Zeb2 have shorter processes and show less branching, respectively (Srivatsa *et al.*, 2015).

To restrain the amount of OB interneurons, about half of the progenitors and young neuroblasts typically undergo programmed cell death during adult neurogenesis (Winner *et al.*, 2002). Apoptosis is typically more frequent upon integration of new neurons into an existing network, such as that of the OB, and failure to receive sensory input triggers cell loss (Corotto, Henegar and Maruniak, 1994; Petreanu and Alvarez-Buylla, 2002; Rochefort *et al.*, 2002). Our results indicate that Zeb2 is required for cell survival in both OB interneuron progenitors in the V-SVZ and in the differentiating interneurons themselves. It remains unclear whether apoptosis is a direct consequence of Zeb2 loss in OB interneurons, or whether the truncated morphology of Zeb2-KO OB interneurons impairs their functional integration and indirectly triggers apoptosis. Loss of Zeb2 itself has also been linked to apoptosis in cancer cell lines as well as during retinal development, where deletion of Zeb2 induces DNA damage-induced apoptosis (Sayan *et al.*, 2009; Qi *et al.*, 2012; Wei *et al.*, 2019).

Zeb2 enables OB interneuron production and maturation via downregulation of *Sox6*

Sox6 is upregulated in the Zeb2-cKO V-SVZ, suggesting that postnatal niche progenitors need to repress *Sox6* to allow for the production of sufficient numbers of correctly specified future OB interneurons. *Sox6* co-determines cell diversification in the telencephalon, substantia nigra and ventral tegmental area during development (Azim *et al.*, 2009; Batista-Brito *et al.*, 2009; Panman *et*

al., 2014). In early postmitotic neurons destined for the cortex (MGE-born), Sox6 acts downstream of Lhx6 and Nkx2-1, regulating tangential migration and distribution, and eventually differentiation and maturation of cortical PV and SST interneurons (Azim *et al.*, 2009; Batista-Brito *et al.*, 2009). Conversely, excessive Sox6 in the Zeb2-cKO V-SVZ might be driving the aberrant appearance of PV+ neuroblast-like cells within the RMS. A similar upregulation of *Sox6* occurs in Zeb2-cKO cortical interneurons, also resulting in defects in interneuron specification, guided migration and maturation (McKinsey *et al.*, 2013; van den Berghe *et al.*, 2013).

Our results clearly show that Sox6 overproduction leads to a decreased neuronal output and aberrant cell shape in the OB, similar to the Zeb2-KO or Zeb2^{ZnF} rescue. *Sox6* transcriptional regulation by Zeb2 is possibly direct, as suggested by ChIP-qPCR. Impaired DNA-binding by the Zeb2^{ZnF} mutant could then also impact on transcriptional repression of *Sox6*, resulting in similar outcomes.

The non-cell-autonomous mode of action of Zeb2

Removing Zeb2 from a large proportion of V-SVZ cells consistently affects non-targeted cells. Within the V-SVZ niche, these cells show a reduction in proliferation as well as an elevation in *Sox6* expression. From our apoptosis study, non-cell-autonomous or indirect effects cannot be deduced in a reliable way due to the low number of CC3+ cells. Nevertheless, in the mutant OB, the numbers of non-targeted 5T4+, CB+ and PV+ cells are significantly reduced, similar to targeted cells. Non-cell-autonomous actions have been documented in the hippocampus anlage, where Zeb2 deletion impacts on proliferation and apoptosis via Wnt signaling. Cell-autonomous versus non-cell-autonomous effects were not further discriminated, however, Sfrp1 (a Wnt antagonist) was upregulated in absence of Zeb2, with most prominent effects on postmitotic cells (Miquelajuregui *et al.*, 2007). In the developing neocortex, an unprecedented, but clear non-cell-autonomous role for Zeb2 has been documented in the timing of neurogenesis and gliogenesis. Via the neurotrophin Ntf3, Zeb2 regulates feedback signaling from postmitotic neurons to progenitors, coordinating the timing of the progenitor cell fate switch (Seuntjens *et al.*, 2009; Parthasarathy *et al.*, 2014). The nature of the non-cell-autonomous actions of Zeb2 in the postnatal V-SVZ remain to be studied in detail.

Zeb2 protein domains control distinct aspects of OB interneuron development

While various roles and action mechanisms downstream of Zeb2 have been documented in many tissues during development, the precise roles of Zeb2 direct interaction with one or more known co-factors have not always been addressed (Van Grunsven *et al.*, 2003; van Grunsven *et al.*, 2007; Verstappen *et al.*, 2008; Wu *et al.*, 2016). Our study is one of the first to show that Zeb2^{WT} protein, and Zeb2^{NIM} and Zeb2^{SBD} mutants bear different rescue capacities in both quantitative and qualitative

terms. A major explanation could be the change in balance between repressor activity of Zeb2 on a set of target genes versus activator activity on another set of genes (for review, see Conidi *et al.*, 2011). This dual role has been observed in neurectoderm differentiation of human ES cells (Chng *et al.*, 2010), embryonic hematopoiesis (Goossens *et al.*, 2011), CNS myelinogenesis (Weng *et al.*, 2012) and adult PNS (Schwann cell mediated) myelination (Quintes *et al.*, 2016; Wu *et al.*, 2016). In these myelinogenesis and (re)myelination studies, Zeb2 generates anti-BMP-Smad and anti-Wnt- β catenin activities where needed, as well as (in adult Schwann Cells) additional anti-Notch and anti-Sox2 activities. Zeb2 is thus clearly a cell differentiation and process regulatory protein that fulfills a role as context-dependent integrator of multiple signaling pathways.

Introducing the Zeb2^{SBD} mutant in the Zeb2cKO|Gsh2 V-SVZ leads to increased numbers of OB interneurons, indicating that Zeb2-Smad cooperation is crucial to tightly regulate the output capacity of niche progenitors. Intriguingly, a similar stronger rescue of neural differentiation is found when a neural induction protocol is applied to mouse Zeb2-KO ES cells overexpressing Zeb2^{SBD} as compared to overexpressing Zeb2^{WT} (Stryjewska, Pieters and Huylebroeck, *unpublished*). This might point towards a more general phenomenon in the context of (neural) stem cells, where Zeb2-Smad interaction inhibits neural differentiation and cell survival. The core motif essential for Zeb2-Smad interaction is a QxVx repeat in a 14 aa-long segment of the initially defined 51 aa-long SBD (Verschueren *et al.*, 1999; Conidi *et al.*, 2013). Mutation of the motif into AxAx made Zeb2 incapable of rescuing the migration defect of Zeb2-KO cortical interneurons and perturbed the dose-dependent downregulation of TGF β /BMP-Smad signaling (Conidi *et al.*, 2013). Therefore, BMP-promoted cell survival may be affected (Grotewold and Rüther, 2002; Sharov *et al.*, 2003). In addition, Smad4, the common-mediator Smad (ten Dijke and Heldin, 2006), is a key regulator of directional progression of postnatal V-SVZ NSCs towards the neuronal lineage (Colak *et al.*, 2008; Kawaguchi-Niida, Shibata and Furuta, 2017). Conditional *Smad4* deletion in V-SVZ progenitors results in an increase of NSC-like properties and differentiation defects (Kawaguchi-Niida, Shibata and Furuta, 2017). We propose that the introduction of Zeb2^{SBD} in a Zeb2-KO background renders the cells incompetent to correctly regulate Smad family signaling, potentially leaving the cells for a longer period in the proliferative phase preceding their differentiation into OB interneurons and preventing apoptosis.

In contrast to the obtained rescue in the Zeb2cKO|Gsh2 V-SVZ by the mutant Zeb2^{SBD}, introduction of the Zeb2^{NIM} mutant leads to a rescue of OB interneuron morphology, but fails to significantly increase cell numbers. Zeb2^{NIM} protein can no longer recruit NuRD (including the subunits HDAC1/2) and results in reduced Zeb2-NuRD mediated transcriptional repression (Verstappen *et al.*, 2008; Wu *et al.*, 2016). This intermediate rescue may be reminiscent of the milder forms of MOWS

caused by mutations in the NIM of Zeb2 (Yoneda *et al.*, 2002; Zweier *et al.*, 2006; Verstappen *et al.*, 2008).

Taken together, our results show that Zeb2, through two of its known domains, is crucial for generating sufficient numbers and proper maturation of OB interneurons. Our study shows for the first time how the respective Zeb2 SBD and NIM domains contribute to fulfilling these roles. However, which direct target genes as well as intact Zeb2-domain dependent genes are affected by the mutation of these respective domains, and whether these domains besides co-determining cell-autonomous actions also contribute to non-cell-autonomous actions of Zeb2, remains to be investigated.

MATERIALS AND METHODS

Animals

All mice were maintained in CD1/Swiss background and kept at KU Leuven according to local ethical committee approval that follows the current Belgian and EU regulations. Mice carrying a floxed *Zeb2* allele (the largest exon 7, equivalent to exon 8 in human) (named as *Sip1*^{f/f} in Higashi *et al.*, 2002) were crossed with Gsh2-Cre (Kessaris *et al.*, 2006; Fogarty *et al.*, 2007), Dlx5/6-Cre-IRES-GFP (Stenman, Toresson and Campbell, 2003) and *RCE*^{f/f}-reporter mice (*R26R*^{CAG-loxP-stop-loxP-eGFP}; Sousa *et al.*, 2009). We refer to the respective genotypes of the mice as indicated in Table 1 (using the Gsh2-Cre approach as example; see also Seuntjens *et al.*, 2009); a similar convention is used for the Dlx5/6-Cre approach.

DNA constructs

Expression vectors used in electroporation experiments were based on pCIG (a pCAGGS-IRES-eGFP plasmid; Megason and McMahon, 2002) obtained via P. Vanderhaeghen (ULB, Brussels) wherein eGFP was replaced by TdTomato. For deleting *Zeb2* from the postnatal V-SVZ in *Zeb2*^{fl/fl} mice, a pCAGGS-Cre vector was used (H. Cremer). Myc-tagged *Zeb2*^{WT} (Verschueren *et al.*, 1999) and the mutants *Zeb2*^{Znf} (Remacle *et al.*, 1999), *Zeb2*^{NIM} (Wu *et al.*, 2016) and *Zeb2*^{SBD} (Conidi *et al.*, 2013) have been described previously. The Sox6 vector was generated by insertion of the blunted Sox6 cDNA coding region (pCMV-3FLAG-Sox6 plasmid (V. Lefebvre) between *NheI* and *Xhol*) into the *SmaI*-cut pCAGGS-TdTomato vector, in-between the pCAGGS promoter and IRES sequences.

Postnatal electroporation

P2 pups were anesthetized by hypothermia and placed under cold light to facilitate visualization of the brain lateral ventricles by transillumination. 1.5 µl of plasmid mix (3 µg/µl DNA, 3% Fast Green) was injected into the left ventricular cavity. Electroconductive gel (Signagel®, Parker Labs) was placed

on both electrode paddles to avoid damaging the pups and achieve successful current flow. Five 100-V electric pulses were applied (50 ms each, with 950 ms intervals), with the positive electrode positioned in the dorso-lateral region for directing DNA to the V-SVZ. After the pulses, the pups were placed on a thermal plate to recover, after which they were returned with their mother.

Tissue processing

Embryonic brains were isolated and washed in ice-cold phosphate-buffered saline (PBS) before overnight fixation in 4% paraformaldehyde in PBS. For all postnatal ages, mice were deeply anesthetized with an intraperitoneal injection of pentobarbital before intracardiac perfusion with ice-cold saline followed by fixative. Afterwards, brains were removed and fixed overnight at 4 °C and then washed in PBS. For electroporation experiments, 100 µm-thick vibratome sections were used. For marker analysis, overnight fixation was followed by progressive dehydration and paraffin-embedding after which 6 µm-thick coronal sections were made.

Immunohistochemistry

Paraffin-embedded brain sections were processed using an automated platform with DABMAP detection kit (DAB stainings Fig. 1F-I) or without detection kit (fluorescent stainings) (Ventana Discovery, Roche). Primary antibodies used were diluted in antibody diluent (Roche) or Pierce™ Immunostain Enhancer (Invitrogen) to enhance fluorescence signal at final concentration: rabbit anti-Sip1 (anti-Zeb2, custom made, 1:1200; Seuntjens *et al.*, 2009), chicken anti-GFP (Abcam ab13870, 1:600), mouse anti-GFAP-Cy3 (Sigma-Aldrich, C9205, 1:300), goat anti-EGFR-biotin (R&D systems BAF1280, 1:60), guinea pig anti-Dcx (Millipore AB2253, 1:300), rabbit anti-Ki67 (NCL-Ki67p, Novocastra, 1:300), rabbit anti-phospho-Histone H3 (Ser10) (Millipore 06-570, 1:300), rabbit anti-Cleaved Caspase-3 (Asp175) (Cell Signaling 9661S, 1:900), rabbit anti-Calretinin (Abcam ab92341, 1:150), rabbit anti-CB (Chemicon AB1178, 1:300), sheep anti-5T4 (Thermo Fisher Scientific PA5-47690, 1:120), rabbit anti-TH (Millipore AB152, 1:300), rabbit anti-PV (Swant PV27, 1:3,000), rabbit anti-Sox6 (Abcam ab30455, 1:300) and mouse anti-Reelin (gift from Dr. A. Goffinet, University of Leuven, Brussel, Belgium, 1:300). Secondary antibodies used were: donkey anti-chicken Alexa 488, donkey anti-goat Cy3, donkey anti-rat Cy3, donkey anti-rabbit Alexa 555, donkey anti-rabbit Alexa 488, donkey anti-guinea pig Cy3, donkey anti-sheep Cy3, streptavidin Alexa 594, donkey anti-chicken biotinSP and donkey anti-rabbit biotinSP (all 1:600, Jackson ImmunoResearch), donkey anti-mouse Alexa 555, donkey anti-rat Alexa 594 and donkey anti-rabbit 594 (all 1:300, Life Technologies). Sections were imaged using a Leica DMR microscope connected to a Spot camera (Visitron Systems) or a Confocal microscope (Leica SP8x).

Vibratome brain slices were preincubated for 1 h with PBS containing 0.3% Triton-X100 (PBST) and 10% normal donkey serum. Primary antibodies (rabbit anti-RFP, Rockland 600-401-379, 1:10,000; chicken anti-GFP, Abcam ab13870, 1:1,000) were added overnight at 4 °C. Following repeated washing in PBST, secondary antibodies (donkey anti-rabbit Alexa 594, Life Technologies, 1:200 and donkey anti-chicken Alexa 488, Jackson ImmunoResearch, 1:500) were applied for 2 h at room temperature. Slices were washed in PBST and mounted in Mowiol. Images were taken with a confocal microscope (Leica SP8x).

Image analysis

The number of GFP+;Dcx+ cells or the marker-driven mean fluorescence intensity (MFI) was quantified using ImageJ (Rueden *et al.*, 2017). Dcx/GFP overlap was measured using ColocalizerPro software. At least three animals were used for each genotype. Results are represented as mean ± SEM. Statistical significance was determined using the Student's *t*-test. The total amount of RFP+, GFP+, or OB interneuron marker+ cells was quantified using the cell counter plugin in Fiji (Schindelin *et al.*, 2012). For electroporation experiments, animals with less than 40 electroporated cells in the V-SVZ on one section were excluded from analysis and all constructs had a similar electroporation efficiency. Process length was also measured in Fiji. At least three animals were used for each genotype and results are represented as mean ± SEM. Statistical significance was determined using the Student's *t* test or, for multiple comparisons, using two-way ANOVA followed by Tukey's multiple comparisons test.

FACS of V-SVZ cells

V-SVZ tissue of Zeb2cKO|Gsh2 and control|Gsh2 brains was isolated in ice-cold HEPES-buffered Leibovitz's L15 medium (Invitrogen) and cut in small pieces. Cells were dissociated by Papain solution (150 ml per brain at 12 units/ml; Sigma) supplemented with DNase-I (30 units/ml; Roche) for 30 min at 37 °C followed by mechanical dispersion, washed twice with Dulbecco's PBS (Lonza) and passed over a 70-mm cell strainer (BD Falcon). Highly fluorescent cells were sorted using an Arial cell sorter (BD Biosciences) for RNA-seq or an SH800S cell sorter (SONY) for qPCR.

qPCR

qPCR was performed on the P5 V-SVZ of 5 Zeb2cKO|Gsh2 and 5 control mice. GFP+ and GFP- cells were sorted in PBS and afterwards lysed overnight in lysis buffer (37.9 mM Tris HCl, 75 mM EDTA, 75.8 mM NaCl, 0.75% SDS) with proteinase K (1 mg/ml, invitrogen). DNA was isolated and qPCR was done in duplicate on a Bio-Rad CFX96 thermo cycler using SYBR Green PCR Master Mix (Sso Advanced Universal SYBR Green supermix, Bio-Rad).

RNA-seq and data analysis

RNA-seq was performed on the P2 V-SVZ of 5 Zeb2cKO|Gsh2 and 6 control mice. Sorted cells were immediately lysed in TRIzol LS (Invitrogen). RNA was extracted using RNeasy Micro kit (QIAGEN). The RNA-seq library was prepared for analysis according to Illumina TruSeq protocols (www.illumina.com). Briefly, poly(A)- RNA was copied into cDNA, end-repaired, (A)-tailed, ligated with adaptors, and enriched by PCR. RNA-seq library stocks were pooled and sequenced for 36-bp using the HiSeq-2000 sequencer. Low-quality single-end reads were first removed using *fastq_quality_filter* (FASTX-Toolkit) and high-standard quality of all data was confirmed with FastQC. Reads were then mapped to the mouse genome GRCm38 using Tophat2 (v2.0.13). A count table for Ensembl-annotated genes was generated with featureCounts (v1.4.6). To assess differentially expressed genes, DESeq2 was used using a pairwise contrast matrix (e.g. control|Gsh2 versus Zeb2cKO|Gsh2). For clustering, the samples were first transformed using the ‘varianceStabilizingTransformation’ from DESeq2, subsequently scaled and centered, and then separated based on Euclidean distance and complete linkage. PCA was applied to reduce dimensionality and visualize the samples in a 2-D space. Read coverage is visualized with the Integrative Genomics Viewer (IGV, Broad Institute). The RNA-seq data have been deposited with GEO and are accessible under record GSE103003.

RT-qPCR

RNA was obtained from FACS-sorted P2 V-SVZ cells and cDNA was made using SuperScript III First-Strand Synthesis System (Invitrogen). qPCR was done in duplicate on a LightCycler 480 (Roche) using SYBR Green PCR Master Mix (Roche).

Chromatin Immunoprecipitation (ChIP)

Zeb2 ChIP was done as described (Wu *et al.*, 2016). Briefly, nuclei were isolated from 10^8 formaldehyde-fixed cells and isolated nuclear lysates were submitted to sonication (BioRuptor Sonicator, 30 sec on, 15 sec off, for altogether 10 min, high amplitude). Centrifuge-cleared sonicated material was then incubated in 1x ChIP buffer (10x: 0.2 M Hepes, 0.2 M NaCl, 0.02 M EDTA). 50 µl of material was stored at -80 °C to be used as input control, the rest was incubated with 7.5 µg of anti-Zeb2 (Santa Cruz H-260) for 16 h at 4 °C. Then, ChIP material was incubated with 50 µl of Protein-A/G plus agarose beads (Santa Cruz SC-2003) rotating for 1 h at 4 °C. DNA-protein complexes were then eluted from the beads with elution buffer (10 mM Tris-HCl pH 8.0, 1% (w/v) SDS) at 65 °C for 15-20 min, gently shaking. Samples were then incubated for 16 h with 50 µl of 5 M NaCl for reverse crosslinking, followed by digestion with 200 µg Proteinase-K and then with 200 µg of RNaseA. DNA

was precipitated and purified using Qiagen's PCR cleanup kit and then stored at -20 °C till being used for qPCR. The primers for qPCR are listed in Table S1.

Acknowledgements

The authors would like to thank Dr. N. Kessaris for providing the Gsh2-Cre mice and K. Campbell and G. Fishell for generously sharing the Dlx5/6-Cre and RCE mouse lines, respectively. We are indebted to V. Lefebvre for the Sox6 cDNA constructs, and M. Götz for tools and advice during the whole study. We thank P. Van Camp for critically reading the manuscript.

Competing interests

The authors have no competing interests to declare.

Funding

AD was supported by a SB Ph.D. fellowship of FWO (Project N.1S19517N). Elke S was supported by a PhD-fellowship of the Agency of Promotion of Science and Technology (IWT). The DH labs were supported by grants from the KU Leuven Research Council (GOA-11/012, DH), Fund for Scientific Research-Flanders (FWO-V; G.0782.14, DH), Belgian Science Policy IAPVII-07 (DH, FG), Hercules Foundation (ZW09-03 InfraMouse, DH) and Erasmus MC start-up funds. Eve S was supported by FWO-V (K1.5.005.14). The LN lab was supported by the F.R.S.-FNRS, Fonds Léon Fredericq, Fondation Simone et Pierre Clerdent, the Queen Elisabeth Medical Foundation, Belgian Science Policy (project IAPVII-20) and ARC (ARC11/16-01). The Leica SP8x confocal microscope was provided by InfraMouse (KU Leuven-VIB) through a Hercules type 3 project (ZW09-03).

Data availability

Data of the RNA sequencing experiment has been submitted to GEO (record number GSE103003).

REFERENCES

- Altman, J. (2011) 'The Discovery of Adult Mammalian Neurogenesis', in *Neurogenesis in the Adult Brain I*. Dordrecht: Springer. doi: 10.1007/978-4-431-53933-9_1.
- Alvarez-Buylla, A. and García-Verdugo, J. M. (2002) 'Neurogenesis in adult subventricular zone', *The Journal of Neuroscience*, 23(3), pp. 629–634. doi: <https://doi.org/10.1523/JNEUROSCI.22-03-00629.2002>.
- Azim, E. et al. (2009) 'SOX6 controls dorsal-ventral progenitor parcellation and interneuron diversity during neocortical development', *Nature neuroscience*, 12(10), pp. 1238–1247. doi: 10.1038/nn.2387.SOX6.
- Batista-Brito, R., MacHold, R., et al. (2008) 'Gene expression in cortical interneuron precursors is prescient of their mature function', *Cerebral Cortex*, 18(10), pp. 2306–2317. doi: 10.1093/cercor/bhm258.
- Batista-Brito, R., Close, J., et al. (2008) 'The distinct temporal origins of olfactory bulb interneuron subtypes', *Journal of Neuroscience*, 28(15), pp. 3966–3975. doi: 10.1523/JNEUROSCI.5625-07.2008.
- Batista-Brito, R. et al. (2009) 'The cell-intrinsic requirement of Sox6 for cortical interneuron development', *Neuron*, 63(4), pp. 466–481. doi: 10.1016/j.neuron.2009.08.005.The.
- Beclin, C. et al. (2016) 'MiR-200 family controls late steps of postnatal forebrain neurogenesis via Zeb2 inhibition', *Scientific Reports*, 6(October), pp. 1–11. doi: 10.1038/srep35729.
- van den Berghe, V. et al. (2013) 'Directed migration of cortical interneurons depends on the cell-autonomous action of Sip1', *Neuron*, 77(1), pp. 70–82. doi: 10.1016/j.neuron.2012.11.009.
- Bjornsson, C. S. et al. (2015) 'It takes a village: constructing the neurogenic niche', *Developmental Cell*. Elsevier Inc., 32(4), pp. 435–446. doi: 10.1016/j.devcel.2015.01.010.
- Blanchart, A., De Carlos, J. A. and López-Mascaraque, L. (2006) 'Time frame of mitral cell development in the mice olfactory bulb', *The Journal of comparative neurology*, 496, pp. 529–543. doi: 10.1002/cne.20941.
- Brill, M. S. et al. (2010) 'Adult generation of glutamatergic olfactory bulb interneurons', *Nature neuroscience*, 12(12), pp. 1524–1533. doi: 10.1038/nn.2416.
- Cacheux, V. et al. (2001) 'Loss-of-function mutations in SIP1 Smad interacting protein 1 result in a syndromic Hirschsprung disease', *Human Molecular Genetics*, 10(14), pp. 1503–1510. doi: 10.1093/hmg/10.14.1503.

Chng, Z. et al. (2010) 'SIP1 Mediates Cell-Fate Decisions between Neuroectoderm and Mesendoderm in Human Pluripotent Stem Cells', *Cell Stem Cell*. Elsevier Ltd, 6(1), pp. 59–70. doi: 10.1016/j.stem.2009.11.015.

Chung, D. W. D. et al. (2014) 'Functional impact of *ZEB1* mutations associated with Posterior Polymorphous and Fuchs' endothelial corneal dystrophies', *Investigative Ophthalmology and Visual Science*, 55(10), pp. 6159–6166. doi: 10.1167/iovs.14-15247.

Colak, D. et al. (2008) 'Adult neurogenesis requires Smad4- mediated bone morphogenic protein signaling in stem cells', *Journal of Neuroscience*, 28(2), pp. 434–446. doi: 10.1523/JNEUROSCI.4374-07.2008.

Conidi, A. et al. (2011) 'Few Smad proteins and many Smad-interacting proteins yield multiple functions and action modes in TGF β /BMP signaling in vivo', *Cytokine & Growth Factor Reviews*. Elsevier Ltd, 22(5–6), pp. 287–300. doi: 10.1016/j.cytogfr.2011.11.006.

Conidi, A. et al. (2013) 'Four amino acids within a tandem QxVx repeat in a predicted extended alpha-helix of the Smad-Binding Domain of Sip1 are necessary for binding to activated Smad proteins', *PLoS ONE*, 8(10), pp. 1–16. doi: 10.1371/journal.pone.0076733.

Corotto, F. S., Henegar, J. R. and Maruniak, J. A. (1994) 'Odor deprivation leads to reduced neurogenesis and reduced neuronal survival in the olfactory bulb of the adult mouse', *Neuroscience*, 61(4), pp. 739–744. doi: 10.1016/0306-4522(94)90397-2.

Díaz-Guerra, E. et al. (2013) 'Transcriptional regulation of olfactory bulb neurogenesis', *The Anatomical Record*, 296, pp. 1364–1382. doi: 10.1002/ar.22733.

ten Dijke, P. and Heldin, C.-H. (2006) *Smad Signal Transduction. Smads in Proliferation, Differentiation and Disease*.

Doetsch, F. and Alvarez-Buylla, A. (1996) 'Network of tangential pathways for neuronal migration in adult mammalian brain', *Proceedings of the National Academy of Sciences*, 93(25), pp. 14895–14900. doi: 10.1073/pnas.93.25.14895.

Doetsch, F., García-Verdugo, J. M. and Alvarez-Buylla, A. (1997) 'Cellular Composition and Three-Dimensional Organization of the Subventricular Germinal Zone in the Adult Mammalian Brain', *The Journal of Neu*, 17(13), pp. 5046–5061. doi: 10.1523/JNEUROSCI.17-13-05046.1997.

Epifanova, E. et al. (2019) 'Role of Zeb2/Sip1 in neuronal development', *Brain Research*. Elsevier B.V., 1705(September 2018), pp. 24–31. doi: 10.1016/j.brainres.2018.09.034.

Figueres-Oñate, M. and López-Mascaraque, L. (2016) 'Adult olfactory bulb interneuron phenotypes identified by targeting embryonic and postnatal neural progenitors', *Frontiers in Neuroscience*, 10(MAY), pp. 1–12. doi: 10.3389/fnins.2016.00194.

Fogarty, M. et al. (2007) 'Spatial Genetic Patterning of the Embryonic Neuroepithelium Generates GABAergic Interneuron Diversity in the Adult Cortex', *Journal of Neuroscience*, 27(41), pp. 10935–10946. doi: 10.1523/JNEUROSCI.1629-07.2007.

Fuentealba, L. C. et al. (2015) 'Embryonic origin of postnatal neural stem cells', *Cell*. Elsevier Inc., 161(7), pp. 1644–1655. doi: 10.1016/j.cell.2015.05.041.

Funahashi, J. et al. (1991) 'Identification of nuclear factor δEF1 and its binding site essential for lens-specific activity of the δ1-crystallin enhancer', *Nucleic Acids Research*, 19(13), pp. 3543–3547. doi: 10.1093/nar/19.13.3543.

Garavelli, L. et al. (2009) 'Mowat-Wilson syndrome: Facial phenotype changing with age: Study of 19 Italian patients and review of the literature', *American Journal of Medical Genetics, Part A*, 149(3), pp. 417–426. doi: 10.1002/ajmg.a.32693.

Garavelli, L. and Mainardi, P. C. (2007) 'Mowat-Wilson Syndrome', *Orphanet Journal of Rare Diseases*, 2(42). doi: 10.1186/1750-1172-2-42.

Goossens, S. et al. (2011) 'The EMT regulator Zeb2/Sip1 is essential for murine embryonic hematopoietic stem/progenitor cell differentiation and mobilization', *Blood*, 117(21), pp. 5620–5630. doi: 10.1182/blood-2010-08-300236.

Gregory-Evans, C. Y. et al. (2004) 'Ocular coloboma and high myopia with Hirschsprung disease associated with a novel ZFHX1B missense mutation and trisomy 21', *American Journal of Medical Genetics, Part A*, 131 A(1), pp. 86–90. doi: 10.1002/ajmg.a.30312.

Grotewold, L. and Rüther, U. (2002) 'The Wnt antagonist Dickkopf-1 is regulated by Bmp signaling and c-Jun and modulates programmed cell death', *EMBO Journal*, 21(5), pp. 966–975. doi: 10.1093/emboj/21.5.966.

Van Grunsen, L. A. et al. (2001) 'SIP1 (Smad interacting protein 1) and delta EF1 (delta-Crystallin Enhancer Binding Factor) are structurally similar transcription repressors', *The Journal of Bone and Joint Surgery*, 83, pp. 40–47.

van Grunsven, L. A. et al. (2007) 'XSip1 neuralizing activity involves the co-repressor CtBP and occurs through BMP dependent and independent mechanisms', *Developmental Biology*, 306(1), pp. 34–49. doi: 10.1016/j.ydbio.2007.02.045.

Van Grunsven, L. A. *et al.* (2003) 'Interaction between Smad-interacting protein-1 and the corepressor C-terminal binding protein is dispensable for transcriptional repression of E-cadherin', *Journal of Biological Chemistry*, 278(28), pp. 26135–26145. doi: 10.1074/jbc.M300597200.

Hack, I. *et al.* (2002) 'Reelin is a detachment signal in tangential chain-migration during postnatal neurogenesis', *Nature Neuroscience*, 5(10), pp. 939–945. doi: 10.1038/nn923.

Hegarty, S. V. *et al.* (2017) 'Zeb2 is a negative regulator of midbrain dopaminergic axon growth and target innervation', *Scientific Reports*, 7(1), pp. 1–11. doi: 10.1038/s41598-017-08900-3.

Hegarty, S. V., Sullivan, A. M. and O'Keeffe, G. W. (2015) 'Zeb2: A multifunctional regulator of nervous system development', *Progress in Neurobiology*. Elsevier Ltd, 132, pp. 81–95. doi: 10.1016/j.pneurobio.2015.07.001.

Heinritz, W. *et al.* (2006) 'A Missense Mutation in the ZFHX1B Gene Associated With an Atypical Mowat–Wilson Syndrome Phenotype', *American Journal of Medical Genetics*, 140A(11), pp. 1223–1227. doi: 10.1002/ajmg.a.31267.

van Helden, M. J. *et al.* (2015) 'Terminal NK cell maturation is controlled by concerted actions of T-bet and Zeb2 and is essential for melanoma rejection', *Journal of Experimental Medicine*, pp. 2–13. doi: 10.1084/jem.20150809.

Higashi, Y. *et al.* (2002) 'Generation of the floxed allele of the SIP1 (Smad-Interacting Protein 1) gene for Cre-mediated conditional knockout in the mouse', *Genesis*, 32(2), pp. 82–84. doi: 10.1002/gene.10048.

Ivanovski, I. *et al.* (2018) 'Phenotype and genotype of 87 patients with Mowat–Wilson syndrome and recommendations for care', *Genetics in Medicine*, 20(9), pp. 965–975. doi: 10.1038/gim.2017.221.

Kawaguchi-Niida, M., Shibata, N. and Furuta, Y. (2017) 'Smad4 is essential for directional progression from committed neural progenitor cells through neuronal differentiation in the postnatal mouse brain', *Molecular and Cellular Neuroscience*. Elsevier Inc., 83, pp. 55–64. doi: 10.1016/j.mcn.2017.06.008.

Kessaris, N. *et al.* (2006) 'Competing waves of oligodendrocytes in the forebrain and postnatal elimination of an embryonic lineage', *Nature Neuroscience*, 9(2), pp. 173–179. doi: 10.1038/nn1620.

Kosaka, K. *et al.* (1998) 'How simple is the organization of the olfactory glomerulus?: The heterogeneity of so-called periglomerular cells', *Neuroscience Research*, 30(2), pp. 101–110. doi: 10.1016/S0168-0102(98)00002-9.

- Kriegstein, A. and Alvarez-Buylla, A. (2009) 'The glial nature of embryonic and adult neural stem cells', *Annual Review of Neuroscience*, 32(1), pp. 149–184. doi: 10.1146/annurev.neuro.051508.135600.
- Lemasson, M., Saghatelian, A. and Lledo, P. (2005) 'Neonatal and adult neurogenesis provide two distinct populations of newborn neurons to the mouse olfactory bulb', *Science*, 25(29), pp. 6816–6825. doi: 10.1523/JNEUROSCI.1114-05.2005.
- Li, J. et al. (2018) 'Transcription factors Sp8 and Sp9 coordinately regulate olfactory bulb interneuron development', *Cerebral Cortex*, 28(9), pp. 3278–3294. doi: 10.1093/cercor/bhx199.
- Lim, D. A. and Alvarez-Buylla, A. (2014) 'Adult neural stem cells stake their ground', *Trends in Neurosciences*. Elsevier Ltd, 37(10), pp. 563–571. doi: 10.1016/j.tins.2014.08.006.
- Lim, D. A. and Alvarez-Buylla, A. (2016) 'The Adult Ventricular–Subventricular Zone (V-SVZ) and Olfactory Bulb (OB) Neurogenesis', *Cold Spring Harb Perspect Biol*, 2(8), pp. 18820–18821. doi: 10.1101/cshperspect.a018820.
- McKinsey, G. L. et al. (2013) 'Dlx1&2-dependent expression of Zfhx1b (Sip1, Zeb2) regulates the fate switch between cortical and striatal interneurons', *Neuron*. Elsevier, 77(1), pp. 83–98. doi: 10.1016/j.neuron.2012.11.035.
- Merkle, F. T. et al. (2014) 'Adult neural stem cells in distinct microdomains generate previously unknown interneuron types', *Nature Neuroscience*, 17(2), pp. 207–214. doi: 10.1038/nn.3610.
- Miquelajuregui, A. et al. (2007) 'Smad-interacting protein-1 (Zfhx1b) acts upstream of Wnt signaling in the mouse hippocampus and controls its formation', *Proceedings of the National Academy of Sciences of the United States of America*, 104(31), pp. 12919–12924. doi: 10.1073/pnas.0609863104.
- Mirzadeh, Z. et al. (2008) 'Neural stem cells confer unique pinwheel architecture to the ventricular surface in neurogenic regions of the adult brain', *Cell Stem Cell*, 3(3), pp. 265–278. doi: 10.1016/j.stem.2008.07.004.Neural.
- Mowat, D. R. et al. (1998) 'Hirschsprung disease, microcephaly, mental retardation, and characteristic facial features: delineation of a new syndrome and identification of a locus at chromosome 2q22-q23', *Journal of medical genetics*, 35(8), pp. 617–23. doi: 10.1136/jmg.35.8.617.
- Okuyama-Yamamoto, A. et al. (2005) 'Changes in reelin expression in the mouse olfactory bulb after chemical lesion to the olfactory epithelium', *European Journal of Neuroscience*, 21(9), pp. 2586–2592. doi: 10.1111/j.1460-9568.2005.04082.x.

Omilusik, K. D. *et al.* (2015) 'Transcriptional repressor ZEB2 promotes terminal differentiation of CD8+ effector and memory T cell populations during infection', *Journal of Experimental Medicine*, pp. 2027–2039. doi: 10.1084/jem.20150194.

Panman, L. *et al.* (2014) 'Sox6 and Otx2 control the specification of substantia nigra and ventral tegmental area dopamine neurons', *Cell Reports*. The Authors, 8(4), pp. 1018–1025. doi: 10.1016/j.celrep.2014.07.016.

Parthasarathy, S. *et al.* (2014) 'Ntf3 acts downstream of Sip1 in cortical postmitotic neurons to control progenitor cell fate through feedback signaling', *Development*, 06, pp. 3324–3330. doi: 10.1242/dev.114173.

Petreanu, L. and Alvarez-Buylla, A. (2002) 'Maturation and death of adult-born olfactory bulb granule neurons: role of olfaction', *The Journal of neuroscience*, 22(14), pp. 6106–6113. doi: 20026588.

Price, J. L. and Powell, T. P. (1970) 'The morphology of the granule cells of the olfactory bulb', *Journal of cell science*, 7(1), pp. 91–123. Available at: <http://www.ncbi.nlm.nih.gov/pubmed/5476864>.

Qi, S. *et al.* (2012) 'ZEB2 mediates multiple pathways regulating cell proliferation, migration, invasion, and apoptosis in glioma', *PLoS ONE*, 7(6), pp. 1–12. doi: 10.1371/journal.pone.0038842.

Quintes, S. *et al.* (2016) 'Zeb2 is essential for Schwann cell differentiation, myelination and nerve repair', *Nature Neuroscience*, 19(8), pp. 1050–1059. doi: 10.1038/nn.4321.

Remacle, J. E. *et al.* (1999) 'New mode of DNA binding of multi-zinc finger transcription factors: deltaEF1 family members bind with two hands to two target sites', *The EMBO journal*, 18(18), pp. 5073–5084. doi: 10.1093/emboj/18.18.5073.

Rochefort, C. *et al.* (2002) 'Enriched Odor Exposure Increases the Number of Newborn Neurons in the Adult Olfactory Bulb and Improves Odor Memory', *Journal of Neuroscience*, 22(7), pp. 2679–2689. doi: 10.1523/jneurosci.22-07-02679.2002.

Rueden, C. T. *et al.* (2017) 'ImageJ2: ImageJ for the next generation of scientific image data', *BMC bioinformatics*. BioMed Central, 18(1), p. 529.

Sayan, A. E. *et al.* (2009) 'SIP1 protein protects cells from DNA damage-induced apoptosis and has independent prognostic value in bladder cancer', *Proceedings of the National Academy of Sciences of the United States of America*, 106(35), pp. 14884–14889. doi: 10.1073/pnas.0902042106.

Schindelin, J. *et al.* (2012) 'Fiji: an open-source platform for biological-image analysis.', *Nature methods*, 9(7), pp. 676–82. doi: 10.1038/nmeth.2019.

Scott, C. L. et al. (2016) 'The transcription factor Zeb2 regulates development of conventional and plasmacytoid DCs by repressing Id2', *The Journal of Experimental Medicine*, 213(6), pp. 897–911. doi: 10.1084/jem.20151715.

Sekido, R. et al. (1994) 'The delta-crystallin enhancer-binding protein delta EF1 is a repressor of E2-box-mediated gene activation.', *Molecular and Cellular Biology*, 14(9), pp. 5692 LP – 5700. doi: 10.1128/MCB.14.9.5692.

Seuntjens, E. et al. (2009) 'Sip1 regulates sequential fate decisions by feedback signaling from postmitotic neurons to progenitors', *Nature Neuroscience*, 12(11), pp. 1373–1380. doi: 10.1038/nn.2409.

Sharov, A. A. et al. (2003) 'Noggin overexpression inhibits eyelid opening by altering epidermal apoptosis and differentiation', *EMBO Journal*, 22(12), pp. 2992–3003. doi: 10.1093/emboj/cdg291.

Sousa, V. H. et al. (2009) 'Characterization of Nkx6-2-derived neocortical interneuron lineages', *Cerebral Cortex*, 19, pp. 1–10. doi: 10.1093/cercor/bhp038.

Srivatsa, S. et al. (2015) 'Sip1 downstream effector ninein controls neocortical axonal growth, ipsilateral branching, and microtubule growth and stability', *Neuron*, 85(5), pp. 998–1012. doi: 10.1016/j.neuron.2015.01.018.

Stenman, J., Toresson, H. and Campbell, K. (2003) 'Identification of two distinct progenitor populations in the lateral ganglionic eminence: implications for striatal and olfactory bulb neurogenesis', *The Journal of neuroscience*, 23(1), pp. 167–174. doi: 23/1/167 [pii].

Stryjewska, A. et al. (2017) 'Zeb2 regulates cell fate at the exit from epiblast state in mouse embryonic stem cells', *Stem Cells*, 35(3), pp. 611–625. doi: 10.1002/stem.2521.

Takahashi, H. et al. (2016) 'A Subtype of Olfactory Bulb Interneurons Is Required for Odor Detection and Discrimination Behaviors', *Journal of Neuroscience*, 36(31), pp. 8210–8227. doi: 10.1523/JNEUROSCI.2783-15.2016.

Urbán, N. and Guillemot, F. (2014) 'Neurogenesis in the embryonic and adult brain: same regulators, different roles', *Frontiers in cellular neuroscience*, 8, pp. 1–19. doi: 10.3389/fncel.2014.00396.

Verschueren, K. et al. (1999) 'SIP1, a novel zinc finger/homeodomain repressor, interacts with Smad proteins and binds to 5'-CACCT sequences in candidate target genes', *Journal of Biological Chemistry*, 274(29), pp. 20489–20498. doi: 10.1074/jbc.274.29.20489.

Verstappen, G. et al. (2008) 'Atypical Mowat-Wilson patient confirms the importance of the novel

association between ZFHX1B/SIP1 and NuRD corepressor complex', *Human Molecular Genetics*, 17(8), pp. 1175–1183. doi: 10.1093/hmg/ddn007.

Waclaw, R. R. et al. (2006) 'The zinc finger transcription factor Sp8 regulates the generation and diversity of olfactory bulb interneurons', *Neuron*, 49(4), pp. 503–516. doi: 10.1016/j.neuron.2006.01.018.

Wakamatsu, N. et al. (2001) 'Mutations in SIP1, encoding Smad interacting protein-1, cause a form of Hirschsprung disease', *Nature Genetics*, 27(4), pp. 369–370. doi: 10.1038/86860.

Wei, W. et al. (2019) 'Requirement of the Mowat-Wilson Syndrome Gene Zeb2 in the Differentiation and Maintenance of Non-photoreceptor Cell Types During Retinal Development', *Molecular Neurobiology*. Molecular Neurobiology, 56(3), pp. 1719–1736. doi: 10.1007/s12035-018-1186-6.

Weng, Q. et al. (2012) 'Dual-mode modulation of Smad signaling by Smad-interacting protein Sip1 is required for myelination in the central nervous system', *Neuron*. Elsevier Inc., 73(4), pp. 713–728. doi: 10.1016/j.neuron.2011.12.021.

Winner, B. et al. (2002) 'Long-term survival and cell death of newly generated neurons in the adult rat olfactory bulb', *European Journal of Neuroscience*, 16, pp. 1681–1689. doi: 10.1046/j.1460-9568.2002.02238.x.

Wu, L. M. N. et al. (2016) 'Zeb2 Recruits HDAC-NuRD to Inhibit Notch and Controls Schwann Cell Differentiation and Remyelination', *Nature Neuroscience*, 19(8), pp. 1060–1072. doi: 10.1002/stem.1868.Human.

Yoneda, M. et al. (2002) 'Late infantile Hirschsprung disease-mental retardation syndrome with a 3-bp deletion in ZFHX1B', *Neurology*, 59(10), pp. 1637–1640. doi: 10.1212/01.WNL.0000034842.78350.4E.

Yoshihara, S. -i. et al. (2012) '5T4 Glycoprotein Regulates the Sensory Input-Dependent Development of a Specific Subtype of Newborn Interneurons in the Mouse Olfactory Bulb', *Journal of Neuroscience*, 32(6), pp. 2217–2226. doi: 10.1523/JNEUROSCI.5907-11.2012.

Young, K. M. et al. (2007) 'Subventricular zone stem cells are heterogeneous with respect to their embryonic origins and neurogenic fates in the adult olfactory bulb', *Journal of Neuroscience*, 27(31), pp. 8286–8296. doi: 10.1523/JNEUROSCI.0476-07.2007.

Zweier, C. et al. (2002) "Mowat-Wilson" syndrome with and without Hirschsprung disease is a distinct, recognizable multiple congenital anomalies-mental retardation syndrome caused by mutations in the zinc finger homeo box 1B gene', *American Journal of Medical Genetics*, 108(3), pp. 177–181. doi: 10.1002/ajmg.10226.

Zweier, C. et al. (2005) 'Clinical and mutational spectrum of Mowat-Wilson Syndrome', *European Journal of Medical Genetics*, 48(2), pp. 97–111. doi: 10.1016/j.ejmg.2005.01.003.

Zweier, C. et al. (2006) 'Atypical ZFHX1B mutation associated with a mild Mowat-Wilson syndrome phenotype', *American Journal of Medical Genetics*, 140A, pp. 869–872. doi: 10.1002/ajmg.a.

Figures

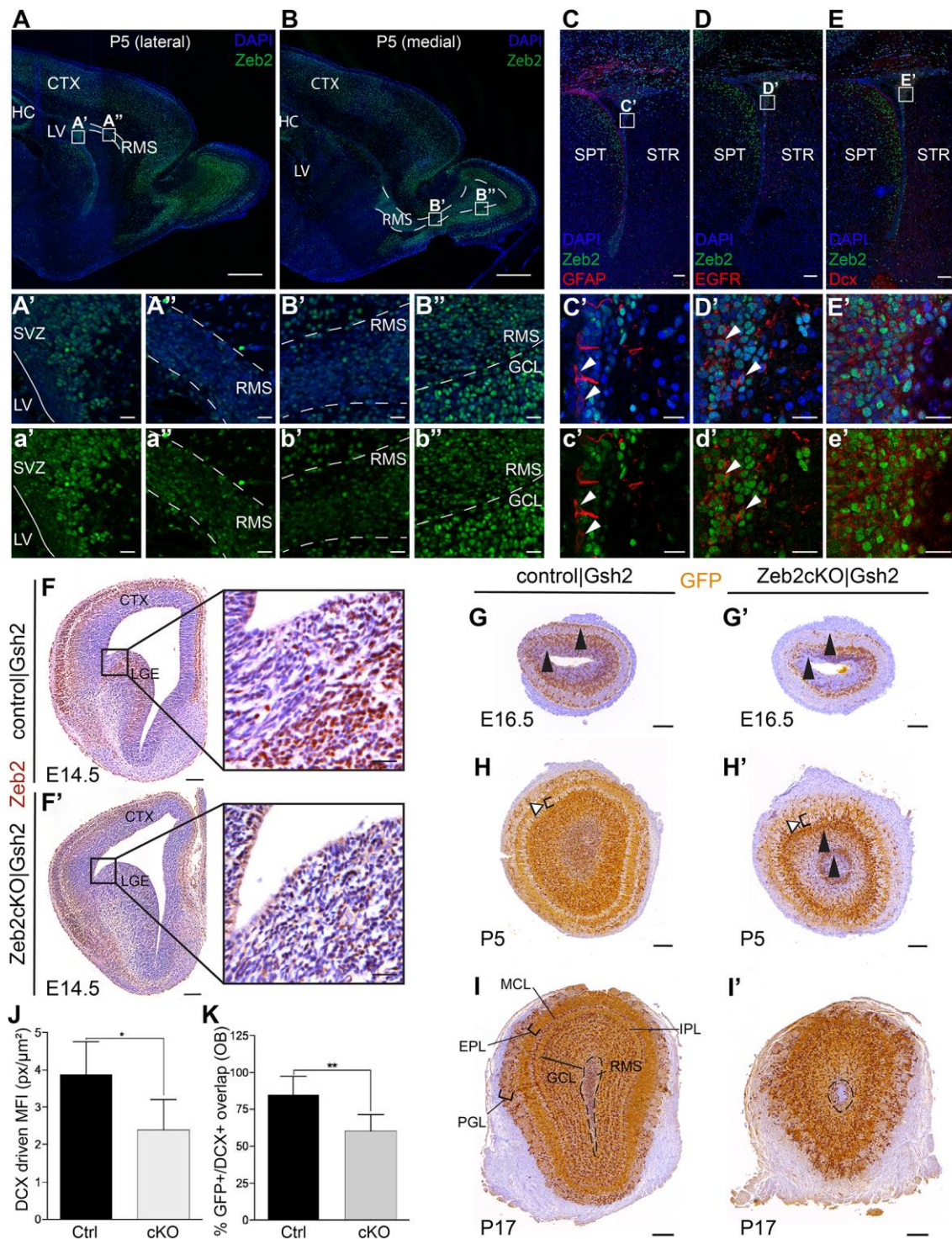


Figure 1. Zeb2 is more prominent in differentiated cells and its genetic inactivation impairs V-SVZ neuroblast output and OB organization.

A-B. Zeb2 immunostaining on wild-type sagittal sections through the telencephalon at P5. Zeb2 levels were high in the V-SVZ (A'), dropped in migrating neuroblasts in the RMS (A'',B') and increased

again in differentiated neurons in the GCL and PGL (B'') (sections stained in one batch and imaged with same settings).

C-E. Zeb2 and GFAP, EGFR or Dcx co-staining on wild-type coronal sections at P5. Zeb2 levels were low in GFAP+ B cells and were upregulated in EGFR+ C cells and Dcx+ A cells (sections stained in one batch and imaged with same settings for Zeb2).

F,F'. Validation of Cre-mediated inactivation of Zeb2 in the Gsh2 model using immunostaining for Zeb2 on coronal E14.5 control|Gsh2 and Zeb2cKO|Gsh2 sections.

G-I. GFP immunohistochemistry showing Gsh2-Cre-targeted cells in control and Zeb2 mutant OBs. At E16.5, Zeb2-KO interneurons cluster together and fail to populate the outer, developing GCL (arrowheads; G,G'). At P5, the GCLs were nearly depleted of GFP+ (Zeb2-KO) cells when compared to controls. Targeted cells cluster in 2 ring-like structures in the mutant compared to control OBs (closed arrowheads; H,H'). The RMS was almost depleted of targeted cells in mutant OBs and their MCL did not mature in a tightly organized, 2-3 cells-thick layer (open arrowheads; H,H'). At P17, the Zeb2cKO|Gsh2 OB is more round and the mean area of cross-section was 70% smaller ($p<0.01$, KO: mean area = 1.68 mm^2 ; control: 2.42 mm^2). Although GFP+ cells had distributed evenly in the GCLs, the typical layered GCL structure was visibly impaired. Furthermore, the IPL appeared invaded by GFP+ cells, whereas normally only few cell bodies are found there. Mitral cells failed to form a smooth, single-cell layer (I,I').

J. DCX-driven mean fluorescent intensity (MFI) in OBs at P5. The MFI was significantly reduced in the Zeb2cKO|Gsh2 versus control|Gsh2 OBs (2.4 ± 0.40 vs 3.9 ± 0.44 pixels/ μm^2 , respectively, two-tailed *t*-test, $p<0.05$, $n=4$). **K.** GFP-Dcx overlap in OBs at P5, highlighting significant reduction in Zeb2cKO|Gsh2 versus control|Gsh2 OBs ($85.1\pm5.5\%$ vs $60.1\pm5.0\%$, respectively, two-tailed *t*-test, $p<0.01$, $n=5$).

Error bars indicate SEM, scale bars represent 500 μm in A-B, 100 μm in C-I and 20 μm in the magnified boxes. Abbreviations: CC, corpus callosum; CTX, cortex; Dcx, doublecortin; EGFR, epidermal growth factor receptor; EPL, external plexiform layer; GCL, granule cell layer; GFAP, glial fibrillary acidic protein; HC, hippocampus; IPL, internal plexiform layer; LGE, lateral ganglionic eminence; LV, lateral ventricle; MCL, mitral cell layer; MGE, medial ganglionic eminence; OB, olfactory bulb; PGL, periglomerular layer; RMS, rostral migratory stream; SPT, septum; STR, striatum; V-SVZ, ventricular-subventricular zone.

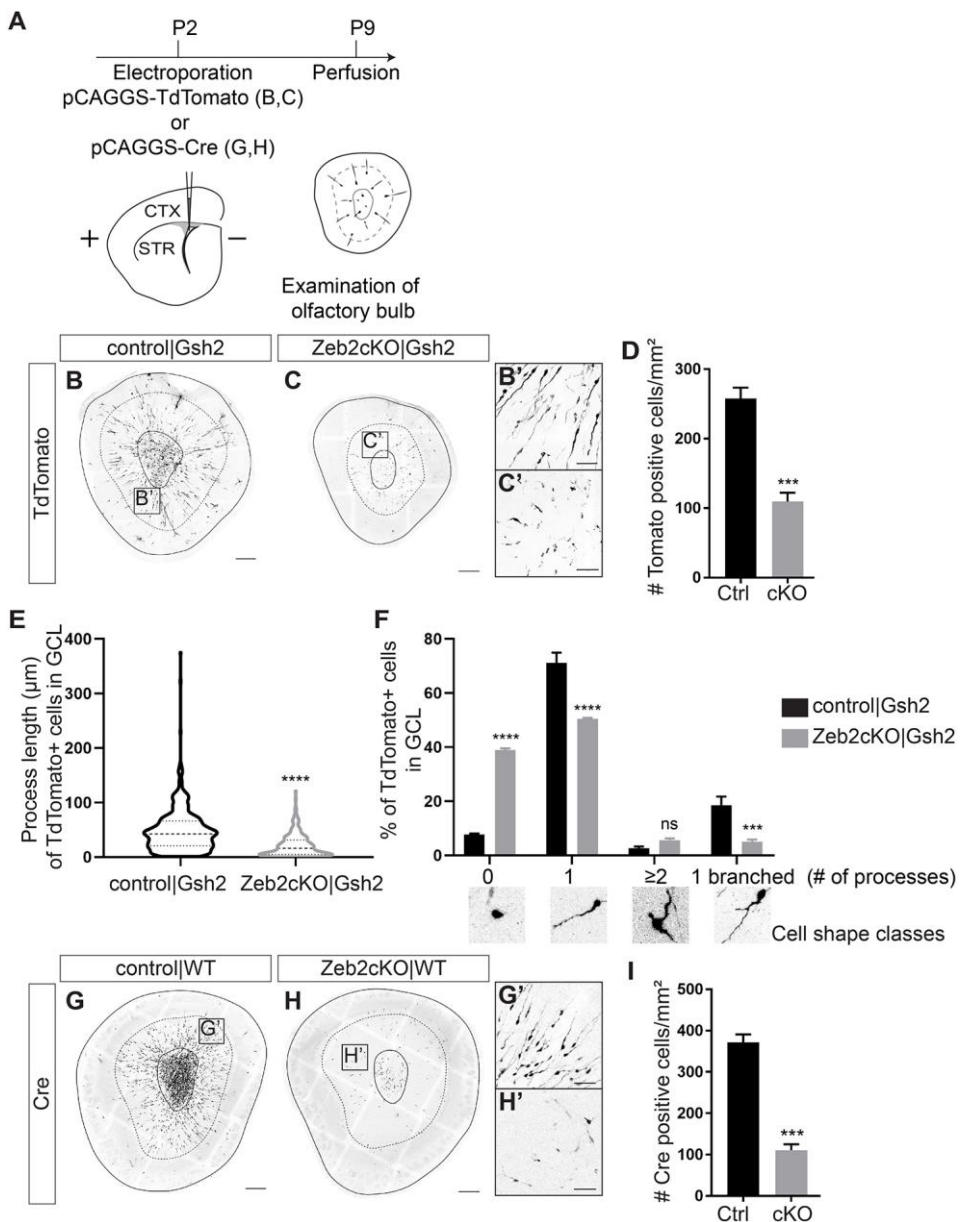


Figure 2. Changes in embryonic and postnatal levels of Zeb2 in the V-SVZ have a major impact on OB interneuron numbers and maturation.

A. Overview of the electroporation experiment. TdTomato- or Cre-vectors were electroporated in V-SVZs at P2. Coronal OB sections were analyzed at P9.

B-C. Embryonic Gsh2-driven *Zeb2* inactivation in the LGE led to a decrease of postnatally generated interneurons in mutants compared to controls. Magnifications B'-C' illustrate aberrant OB interneuron morphology in knockout mice. **D.** Quantification of the number of TdTomato+ cells/mm² in OBs at P9 (control 257.7±15.7 vs cKO 109.3±12.9, two-tailed *t*-test, *p*=0.001, *n* = 4 for control and *n* = 3 for cKO).

E-F. Morphological measurements of TdTomato+ cells in the GCLs of the OB at P9. Violin plot showing process length (from soma to end of the neurite) measured in μm (E). Mean process length is represented by the dashed line and quartiles by dotted lines (mean in control 48.39 μm (434 cells) vs cKO 21.33 μm (242 cells), two-tailed *t*-test, $p<0.0001$). Leading process number sprouting (away from the RMS) from each soma and branching of the process (F). In the knockout, more interneurons without processes (7.742 in control vs 38.89 % in cKO, $p<0.0001$), less interneurons with one process (50.39 in control vs 20.69 % in cKO, $p<0.0001$) and less interneurons with a branched process (18.55 in control vs 5.06 % in cKO, $p<0.01$) were observed. Representative images of each cell shape class are shown under the graph. The total amount of quantified cells is 1453 for control and 574 for cKO, each measured in 3 independent animals (two-way ANOVA).

G-H. Acute postnatal inactivation of Zeb2 in the V-SVZ led to a similar phenotype. Magnifications G'-H' show that postnatal loss of Zeb2 also results in aberrant OB interneuron morphology. **I.**

Quantification of the number of Cre-induced GFP+ cells/ mm^2 in OBs at P9 (control 371.4 ± 19.7 vs cKO 110.8 ± 14.2 , two-tailed *t*-test, $p < 0.001$, $n = 3$ for control and cKO).

Error bars indicate SEM, scale bars represent 200 μm in B,C,G,H and 50 μm in B',C',G',H'.

Abbreviations as in Figure 1.

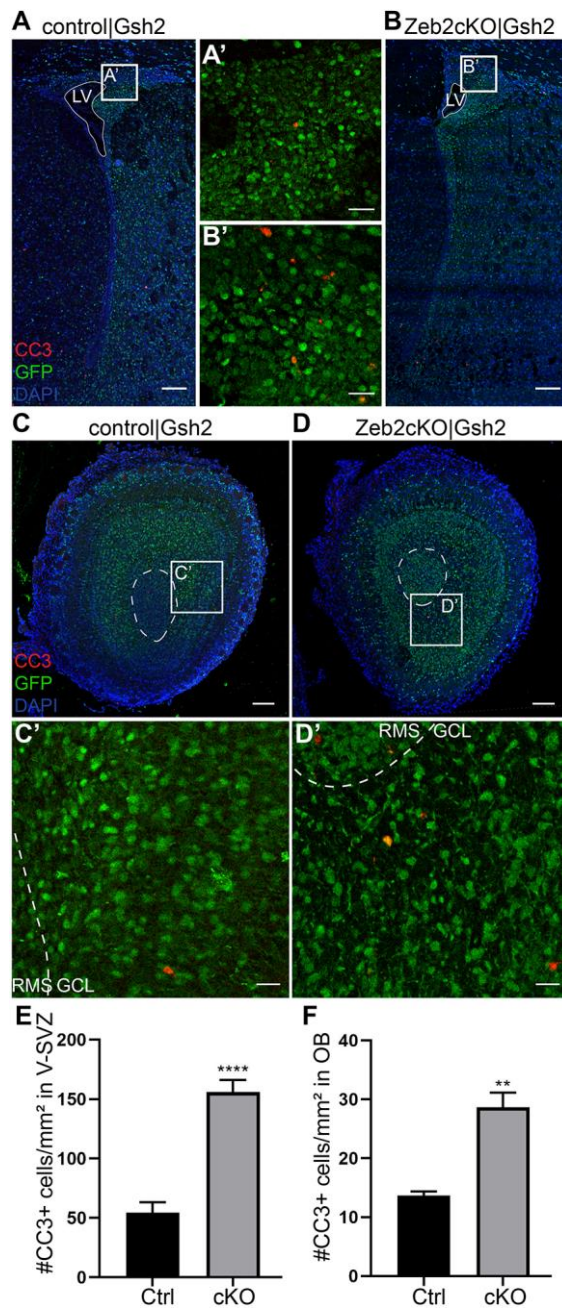


Figure 3. Apoptosis is increased in the postnatal V-SVZ and OB in absence of Zeb2.

A-B. Analysis of apoptosis (Cleaved-Caspase 3, CC3 immunostaining) on coronal sections at P5. The number of CC3+ cells is significantly increased in the Zeb2cKO|Gsh2 V-SVZ compared to control (quantification in E: 55.4 in control vs 155.9 cells/mm² in cKO, two-tailed t-test, p<0.0001, n=8). **C-D.** A similar increase is found in the Zeb2cKO|Gsh2 OB compared to control (quantification in F : 13.6 in control vs 28.7 cells/mm² in cKO, two-tailed t-test, p<0.01, n=3).

Error bars indicate SEM, scale bars represent 100 µm in A-D and 20 µm in magnified boxes.

Abbreviations as in Figure 1.

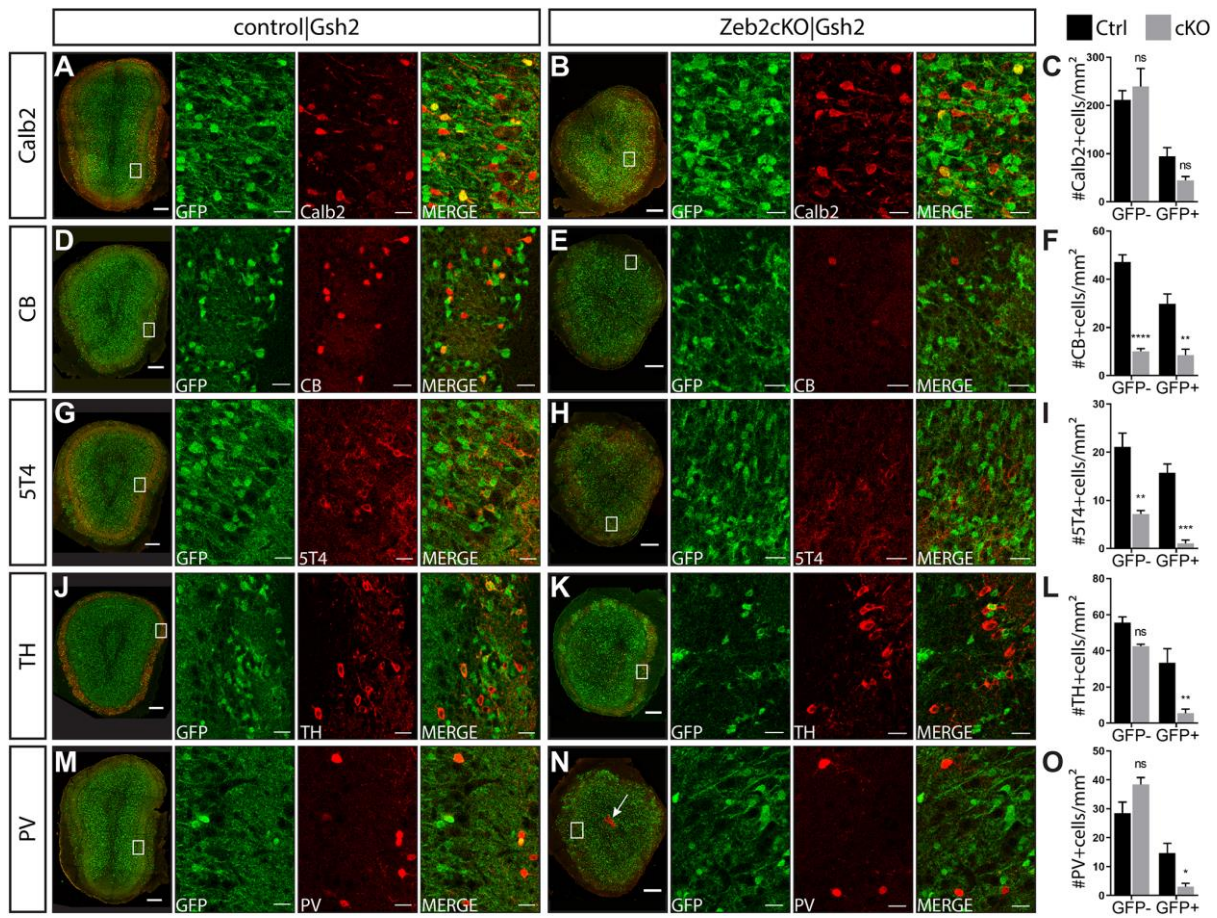


Figure 4. Zeb2 steers differentiation and distribution of distinct OB interneuron subtypes in a cell-autonomous and non-cell-autonomous manner.

Characterization of OB interneuron types at P18 in control|Gsh2 and Zeb2cKO|Gsh2 mice. Relative to OB size, the number of Calb2+ cells did not change, whereas the numbers of CB+ and 5T4+ cells decreased in both the targeted (GFP+) as well as the non-targeted (GFP-) population in Zeb2cKO|Gsh2 mice compared to the control. A decrease in the TH+ and PV+ targeted population can also be observed in the Zeb2cKO|Gsh2 mice. For PV, a particular misplacement of non-targeted cells was found in the Zeb2cKO|Gsh2 RMS (arrow) (1% of PV+ cells in control vs 43% in cKO, p<0.01).

All quantifications are listed as control|Gsh2 vs Zeb2cKO|Gsh2 in number of maker+ cells/mm² (two-way ANOVA). **Calb2:** GFP-: 221.6 vs 238.9, p=0.68, GFP+: 94.71 vs 44.64, p=0.30; **CB:** GFP-: 47.09 vs 10.06, p<0.0001, GFP+: 29.68 vs 8.48, p<0.01; **5T4:** GFP-: 21.09 vs 7.16, p<0.01, GFP+: 15.74 vs 1.08, p<0.001; **TH:** GFP-: 55.64 vs 42.65, p=0.13, GFP+: 33.43 vs 5.48, p<0.01; **PV:** GFP-: 28.53 vs 38.40, p=0.08, GFP+: 14.65 vs 3.07, p<0.05; n=3 for all groups.

Error bars indicate SEM, scale bars represent 200 µm in the overview and 20 µm in the insets.

Abbreviations: 5T4, oncofetal trophoblast glycoprotein; Calb2, calretinin; CB, calbindin; PV, parvalbumin; SST, somatostatin; TH, tyrosine hydroxylase.

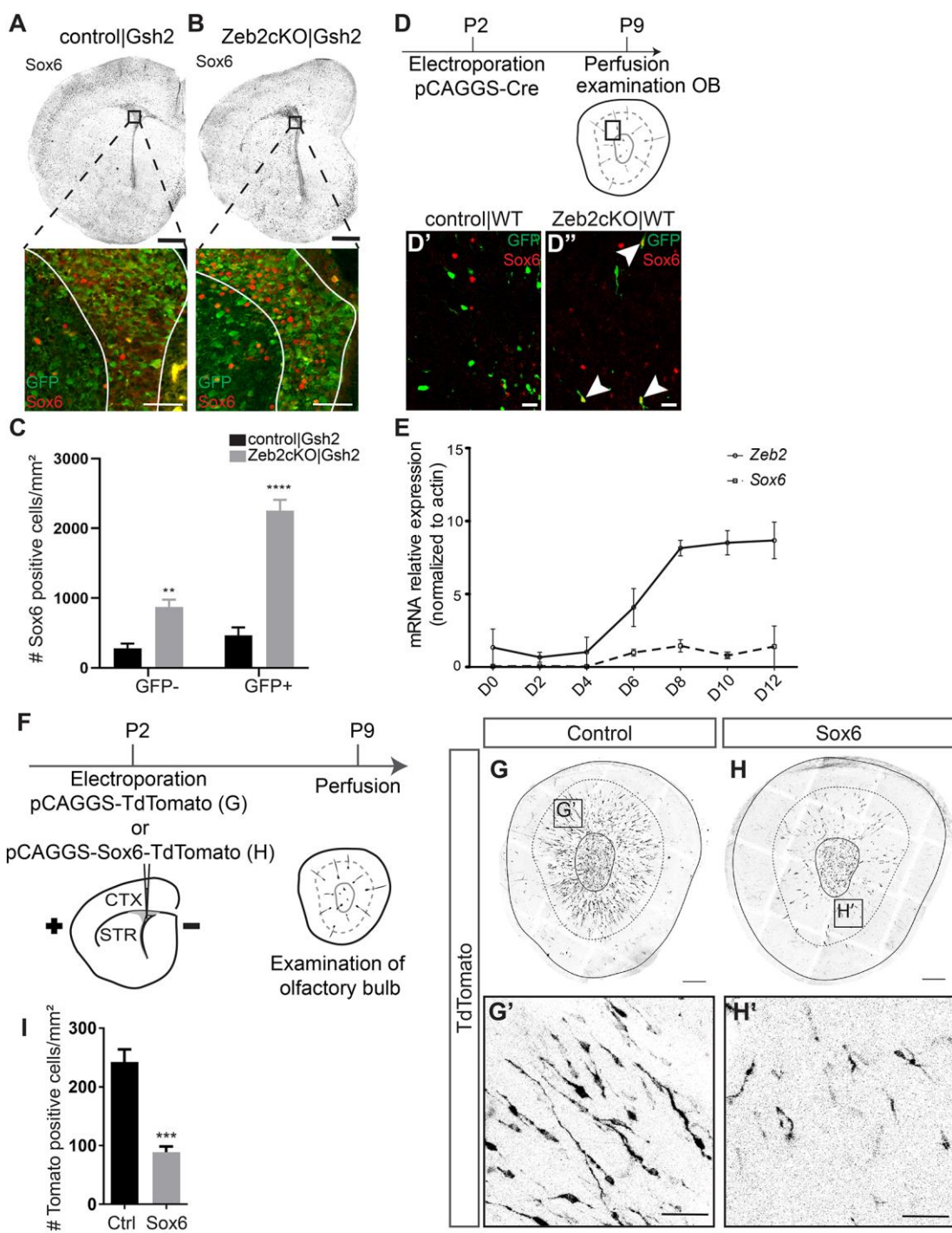


Figure 5. Sox6 is strongly upregulated in the Zeb2cKO|Gsh2 V-SVZ and postnatal overproduction of Sox6 in the V-SVZ mimics loss of Zeb2.

A-B. Staining for Sox6 at P5 in control and mutant V-SVZ. A representative image for GFP and Sox6 is shown in which the increase of Sox6 in both GFP+ and GFP- cells is illustrated. Scale bars represent 200 µm in overview images and 20 µm in magnifications. **C.** Number of Sox6+ cells in the control|Gsh2 and Zeb2cKO|Gsh2 V-SVZ (for GFP-: 281.3 in control vs 873.2 cells/mm² in cKO, p<0.01; for GFP+: 462.9 in control vs 2254 cells/mm² in cKO, two-way ANOVA, p<0.0001, n=5).

- D.** Coronal section through the P9 OB after electroporation of a pCAGGS-Cre construct in the V-SVZ at P2. Boxed area in the OB indicates the magnified region, showing a clearly elevated level of Sox6 in targeted cells upon acute *Zeb2* inactivation. Scale bars represent 20 μ m.
- E.** Normalized expression of *Zeb2* and *Sox6* after ChIP in mouse ESCs subjected to neural differentiation. *Zeb2* and *Sox6* mRNA levels started increasing from D4 of differentiation onwards.
- F.** TdTomato- or *Sox6*-TdTomato-encoding vectors were electroporated in the wild-type (WT) V-SVZ at P2. Coronal OB sections were analyzed at P9.
- G-H.** Overproduction of *Sox6* in the normal V-SVZ led to a significant decrease in neuroblasts that arrived in the OB compared to the control. Magnifications G'-H' show that cells that overproduced *Sox6* have a smaller cell body and thinner processes and have a defect in laminar organization. Scale bars represent 200 μ m in G,H and 50 μ m in G',H'. **I.** Number of TdTomato+ cells/mm² in the OB at P9 (242.7 \pm 21.2 cells/mm² in control vs 89.0 \pm 9.7 cells/mm² in excess *Sox6*, two-tailed *t*-test, p <0.001, n =5 for control and n =9 for excess *Sox6*).

Error bars indicate SEM. Abbreviations as in Figure 1.

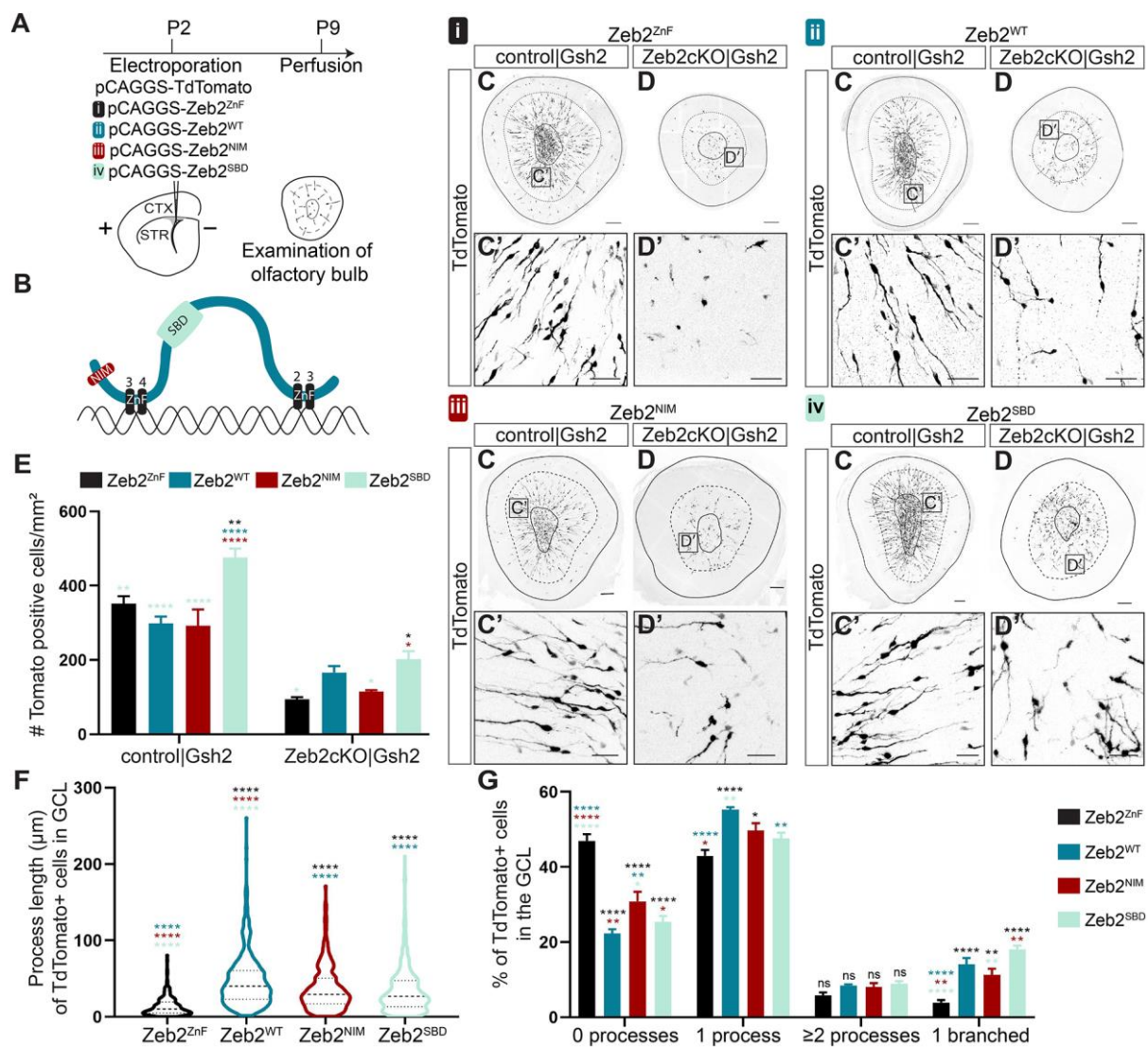


Figure 6. Zeb2 domains contribute differently to neuroblast generation and maturation.

A. Schematic representation of electroporation of TdTomato- together with Zeb2^{WT}, Zeb2^{ZnF}, Zeb2^{SBD} or Zeb2^{NIM}-encoding vectors at P2 in V-SVZ. Coronal OB sections were analyzed at P9. **B.** Schematic representation of Zeb2, bound to DNA via specific zinc fingers in NZF and CZF. The NIM is located at the N-terminus, the SBD is present between the two ZnF domains.

C-D. Postnatal reintroduction of Zeb2 in control and Zeb2cKO|Gsh2 V-SVZ. Zeb2^{ZNF} mutant phenocopied the *Zeb*-cKO. Reintroduction of wild-type Zeb2 (Zeb2^{WT}), Zeb2^{SBD} or Zeb2^{NIM} mutant protein affected the number of cells reaching the OB as well as their morphology.

E. Quantification of the relative amount of OB interneurons (numbers of TdTomato+ cells/mm², two-way ANOVA) at P9. Only reintroduction of Zeb2^{WT} or Zeb2^{SBD} resulted in an increase in the number of OB interneurons compared to Zeb2^{ZNF} (Zeb2^{WT}: p=0.15, Zeb2^{SBD}: p=0.01). Overexpression of Zeb2^{SBD} in control|Gsh2 mice significantly raised the number of neurons that migrate to the OB (vs Zeb2^{ZNF} p<0.01, vs Zeb2^{WT} p<0.0001, vs Zeb2^{NIM} p<0.0001). **Zeb2^{ZNF}:** control|Gsh2 351.5 cells/mm² (n=4);

Zeb2cKO|Gsh2 93.87 cells/mm² (n=3), **Zeb2^{WT}**: control|Gsh2 298.3 cells/mm² (n=4); Zeb2cKO|Gsh2 166.7 cells/mm² (n=3), **Zeb2^{NIM}**: control|Gsh2 292.7 cells/mm² (n=3); Zeb2cKO|Gsh2 115.2 cells/mm² (n=4), **Zeb2^{SBD}**: control|Gsh2 476.3 cells/mm² (n=4); Zeb2cKO|Gsh2 202.1 cells/mm² (n=3).

F-G. Morphological measurements of TdTomato+ cells in the GCLs of the OB at P9. Violin plot showing process length (from soma to end of the neurite) measured in µm (F). Zeb2^{SBD} as well as Zeb2^{NIM} partially rescue, whereas Zeb2^{WT} rescued significantly more the neurite length. Mean process length is represented by the dashed line and quartiles by dotted lines. Mean process length for all constructs: **Zeb2^{ZnF}** 13.64 µm (242 cells), **Zeb2^{WT}** 48.05 µm (389 cells), **Zeb2^{NIM}** 36.85 µm (312 cells), **Zeb2^{SBD}** 34.87 µm (532 cells). All constructs differ significantly (two-way ANOVA, p<0.0001) from one another except Zeb2^{NIM} and Zeb2^{SBD} which showed similar process lengths.

Leading process number sprouting (away from the RMS) from each soma and branching of the process (G). All rescue constructs showed less cells without sprouting and more cells with one (branched) process compared to the Zeb2^{ZnF} control. The Zeb2^{NIM} construct was less potent in rescuing the number of cells without process compared to Zeb2^{WT} (p<0.01) and Zeb2^{SBD} (p<0.05) and had less branched processes compared to the Zeb2^{SBD} (p<0.01), but not Zeb2^{WT}. The total amount of cells quantified are 727, 1327, 845 and 1598 cells for ZnF, WT, NIM and SBD constructs, respectively; all from at least 3 animals (two-way ANOVA).

Error bars indicate SEM, scale bars represent 200 µm in C,D and 50 µm in C',D'. Abbreviations: CTX, cortex; NIM, NuRD interaction motif; OB, olfactory bulb; SBD, Smad binding domain; STR, striatum; SVZ, subventricular zone; ZnF, Zinc Finger.

Tables

Table 1. Terminology of mouse genotypes (using the *Gsh2-Cre* based approach as example)

Genotype	Terminology
<i>Gsh2</i> ^{Cre+} ; <i>Zeb2</i> ^{f/f} / <i>wt</i>	control Gsh2
<i>Gsh2</i> ^{Cre+} ; <i>Zeb2</i> ^{f/f} / <i>ko</i>	Zeb2cKO Gsh2
<i>Gsh2</i> ^{Cre-} ; <i>Zeb2</i> ^{f/f} / <i>wt</i>	control WT
<i>Gsh2</i> ^{Cre-} ; <i>Zeb2</i> ^{f/f} / <i>ko</i>	Zeb2cKO WT

SUPPLEMENTAL FIGURES

Figure S1. Zeb2 expression in the embryonic and postnatal telencephalon

A-D. Zeb2 immunohistochemistry on coronal brain sections (with developmental times given on top of each panel) of the LGE (A) and the V-SVZ (B-D) of control mice. **E-H.** Coronal sections through the developing OB showing the presence of Zeb2 protein in the different cell layers. **I-I'**. Immunostaining for Zeb2 and Reelin in the wild type P5 OB showing absence of co-expression.

Scale bars always represent 100 µm. Abbreviations: CC, corpus callosum; CTX, cortex; EPL, external plexiform layer; GCL, granule cell layer; IPL, internal plexiform layer; LGE, lateral ganglionic eminence; LV, lateral ventricle; MCL, mitral cell layer; MGE, medial ganglionic eminence; PGL, periglomerular layer; RMS, rostral migratory stream; SPT, septum; STR, striatum; V-SVZ, ventricular-subventricular zone.

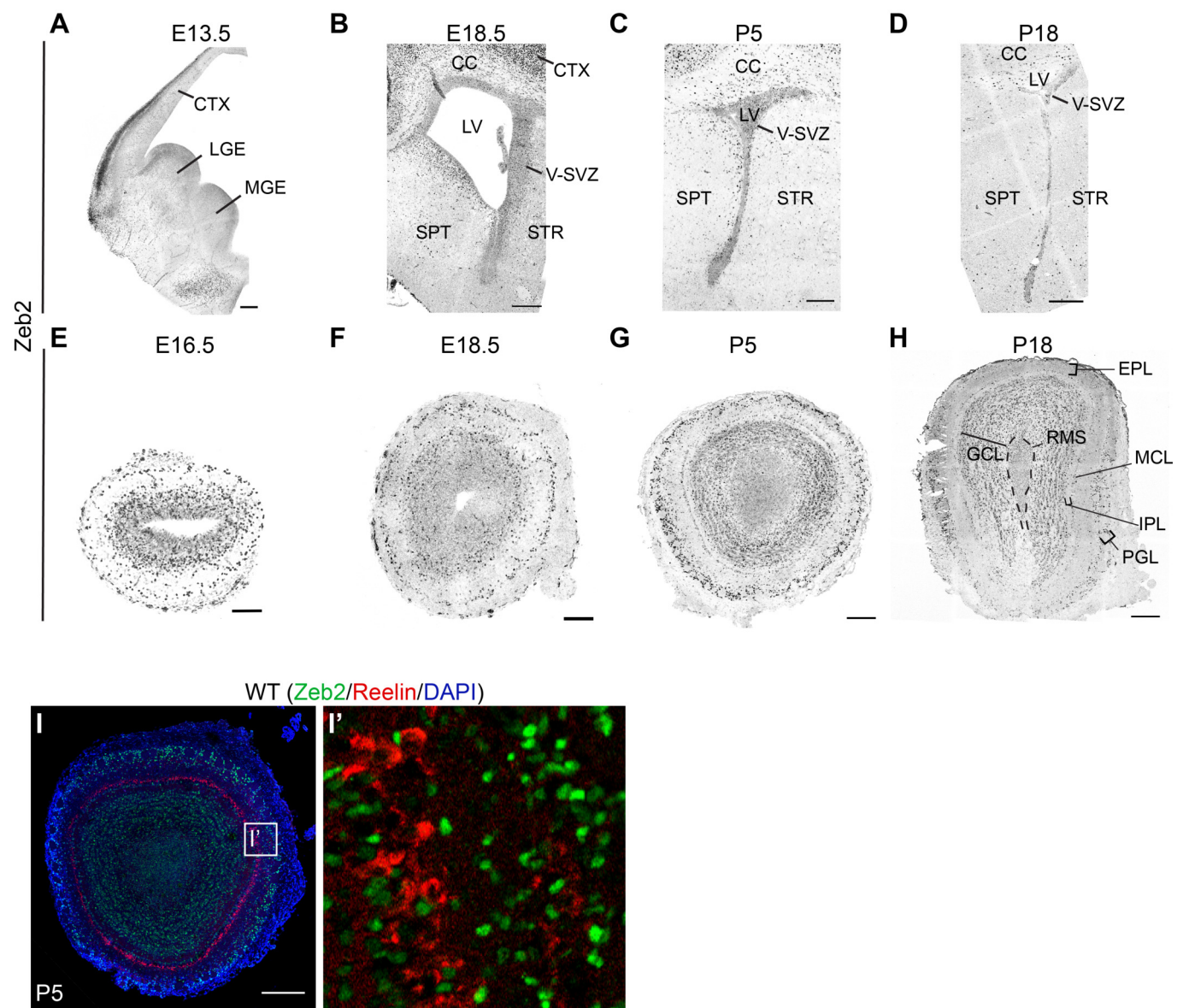


Figure S2. RNA-seq validation

A. Integrative Genomics Viewer (IGV) views of the Zeb2 locus showing the near absence of reads encompassing exon7 in the *Zeb2*-cKO samples (boxed in pink).

B-C. Clustering (B) and PCA analysis (C) indicating that control|Gsh2 and *Zeb2*cKO|Gsh2 samples are clearly distinguishable.

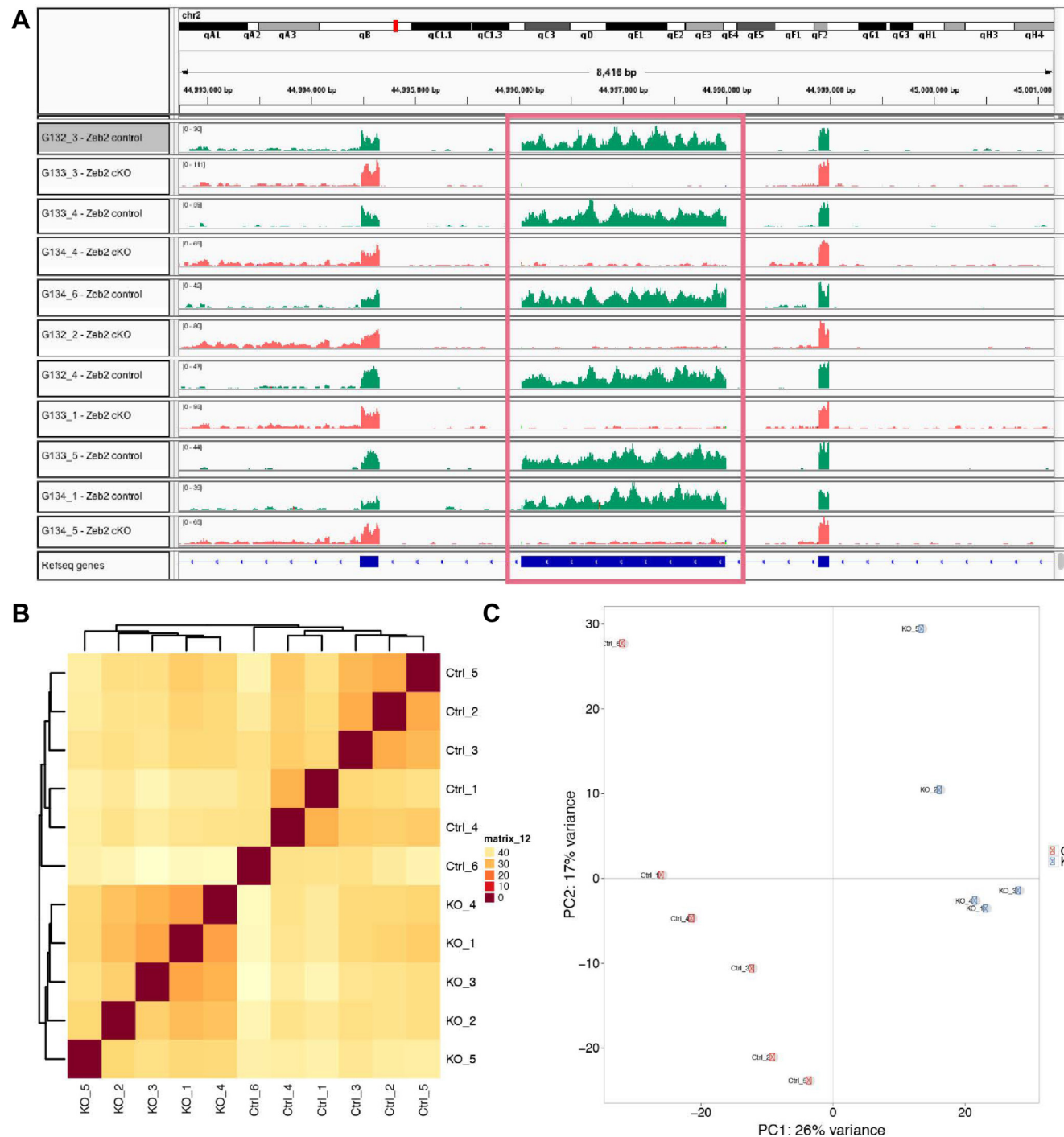


Figure S3. Validation of Zeb2 cKO in the Gsh2 deletion model

A-B. Coronal sections through the P5 Zeb2cKO|Gsh2 and control telencephalon immunostained for Zeb2 and GFP, illustrating efficient Zeb2 removal from the V-SVZ leaving only very few GFP+;Zeb2+ cells in the V-SVZ (white arrowheads). **C.** Normalized expression of the Zeb2 KO construct amounted 0.0087 in GFP+ Zeb2cKO|Gsh2 cells (1 KO allele and 1 Cre mediated cKO allele), 0.0034 in GFP- Zeb2cKO|Gsh2 cells (1 KO allele), 0.0032 in GFP+ control|Gsh2 cells (1 Cre mediated cKO allele) and 0.0003 in GFP- control|Gsh2 cells (no KO allele). The ratios correspond to the genotype, thus ruling out inefficient production of GFP in KO cells.

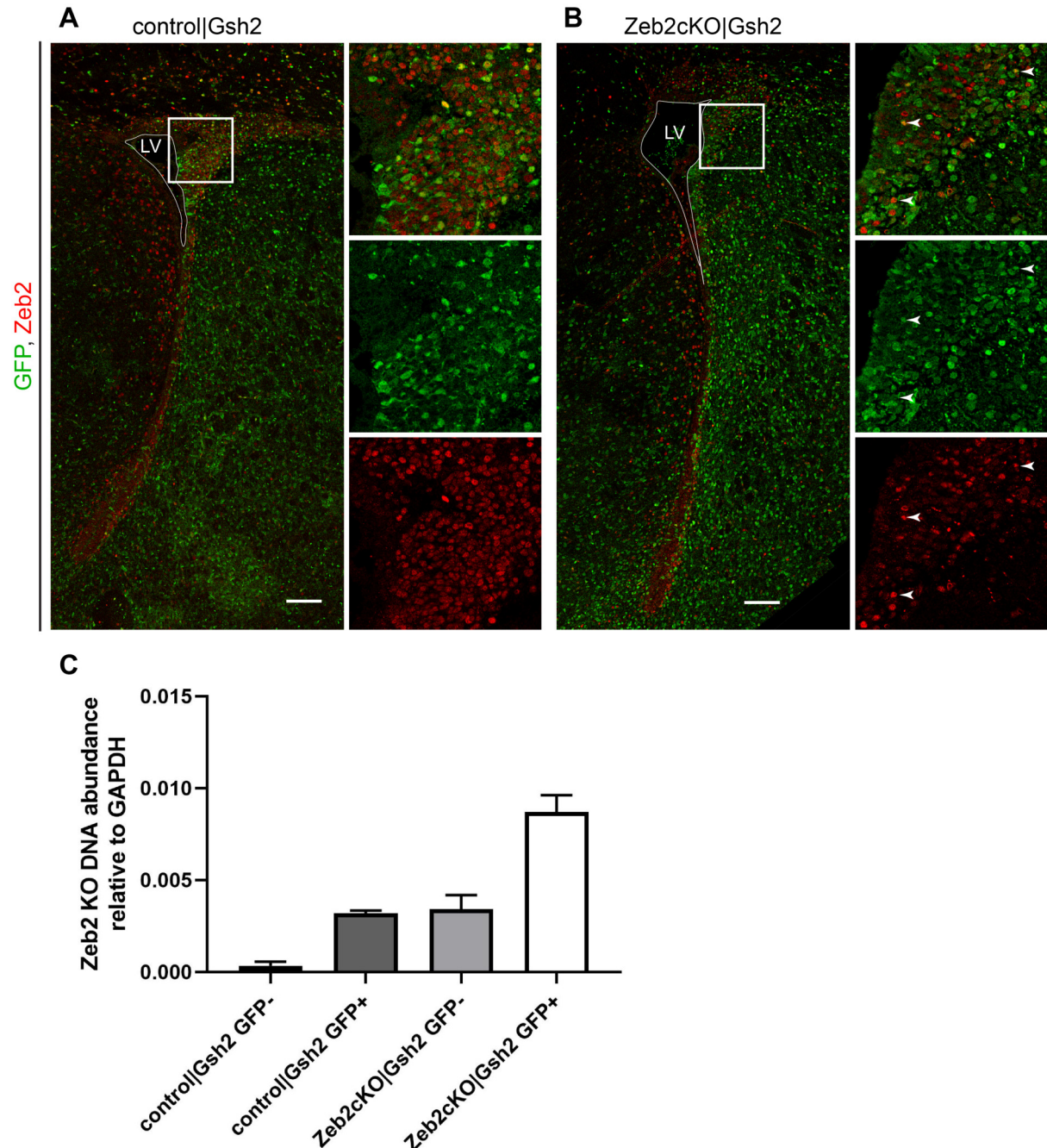


Figure S4. The mitral cells do not produce Zeb2, but fail to form a smooth, single cell layer in the Zeb2cKO|Gsh2 OB

A-F. Coronal section through the Zeb2cKO|Gsh2 and control OB at developmental (A-B) and early postnatal stages (C-F) showing the Reelin+ MCL. Mitral cells can still be found in the Zeb2-KO, but they failed to form a smooth, single-cell layer. Boxed areas represent the magnified region in A'-F'. **G.** Coronal section through a WT OB at P5 showing absence of Zeb2 in the mitral cells (Reelin+). Boxed area represents the magnified region in G'. Scale bars represent 200 μ m. Abbreviations: GCL, granule cell layer; MCL, mitral cell layer; V, ventricle.

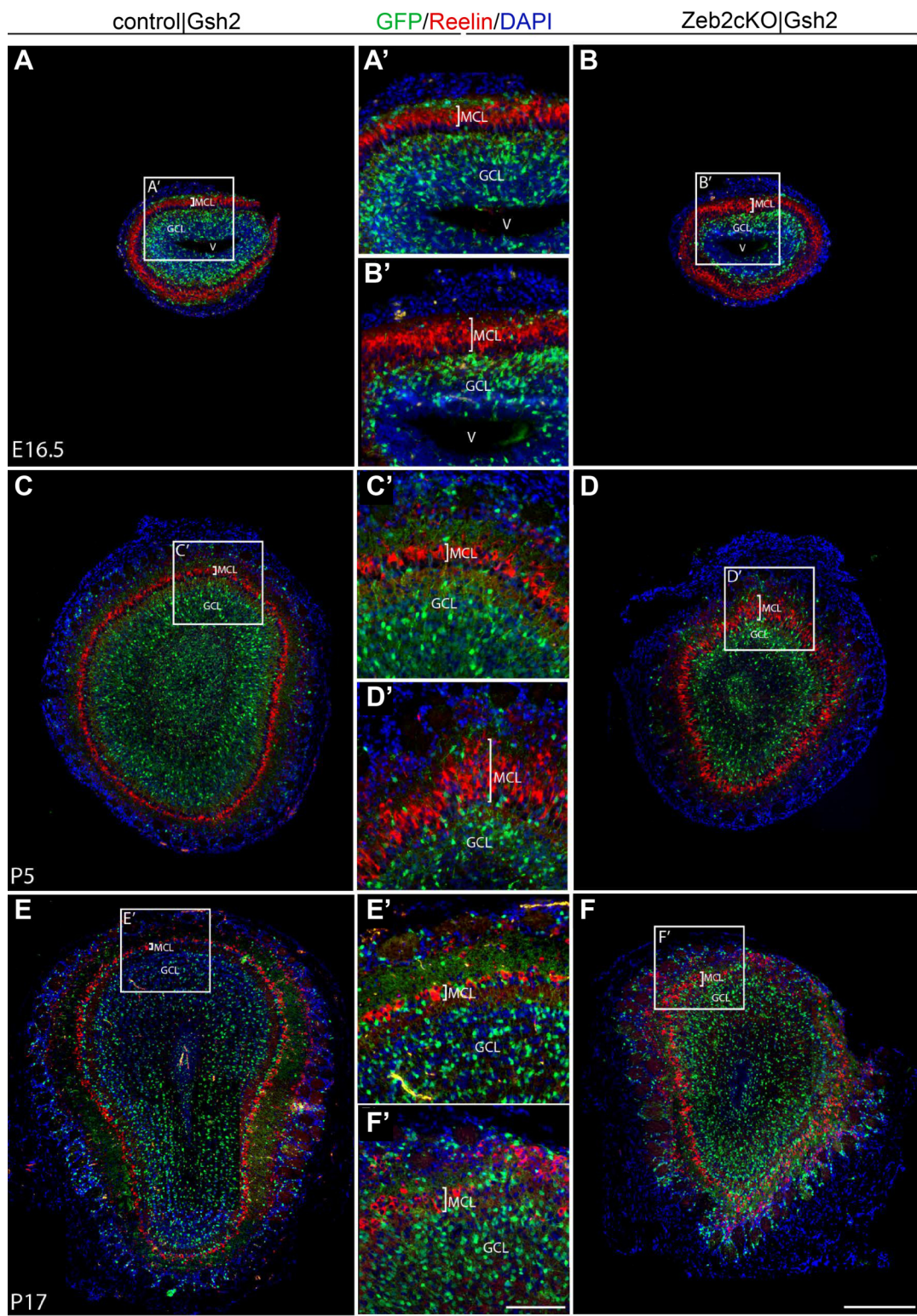


Figure S5. V-SVZ derived Zeb2-depleted cells are not delayed in vivo

- A.** Cre-vector electroporation in the $Zeb2^{fl/wt}$ (control|WT) and $Zeb2^{fl/KO}$ (Zeb2cKO|WT) V-SVZ at P2. Coronal sections of the mutant and control OB were analyzed 54 dpe.
- B.** Significantly less GFP+ cells were found in the WT|Zeb2cKO compared to the control OB.

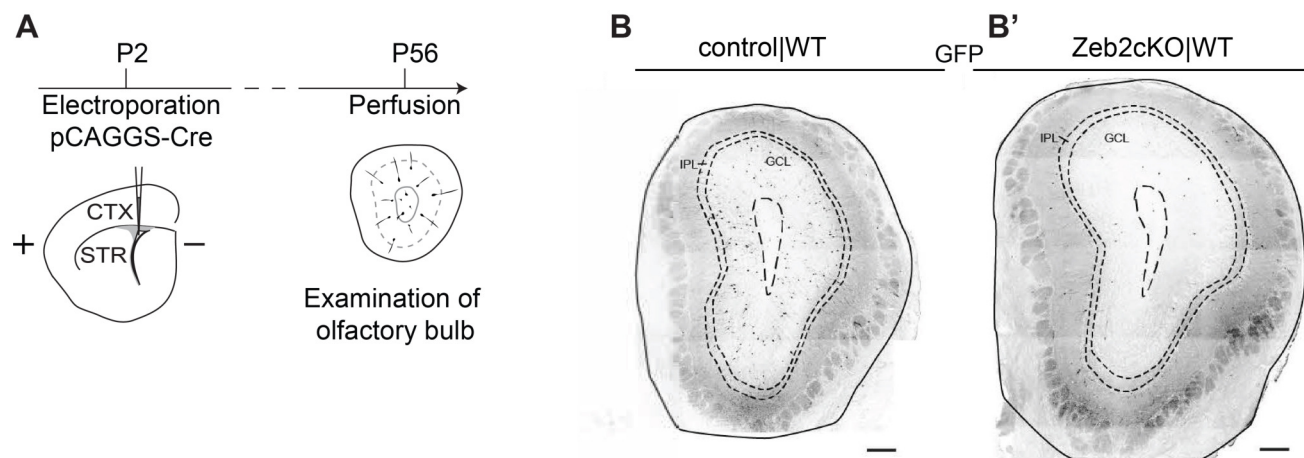


Figure S6. Zeb2 deletion in either Gsh2 or Dlx5/6 progenitors results in underdeveloped olfactory bulbs.

A-D. Immunohistochemistry for GFP and Zeb2 in coronal sections through control (A,C) and *Zeb2*-cKO (B,D) OBs at E18.5. The staining confirms Zeb2 removal in targeted (GFP+) cells. Development of *Dlx5/6*|*Zeb2*cKO OBs is disturbed in a similar way compared to *Zeb2*cKO|*Gsh2* OBs.
Scale bars always represent 100 μ m.

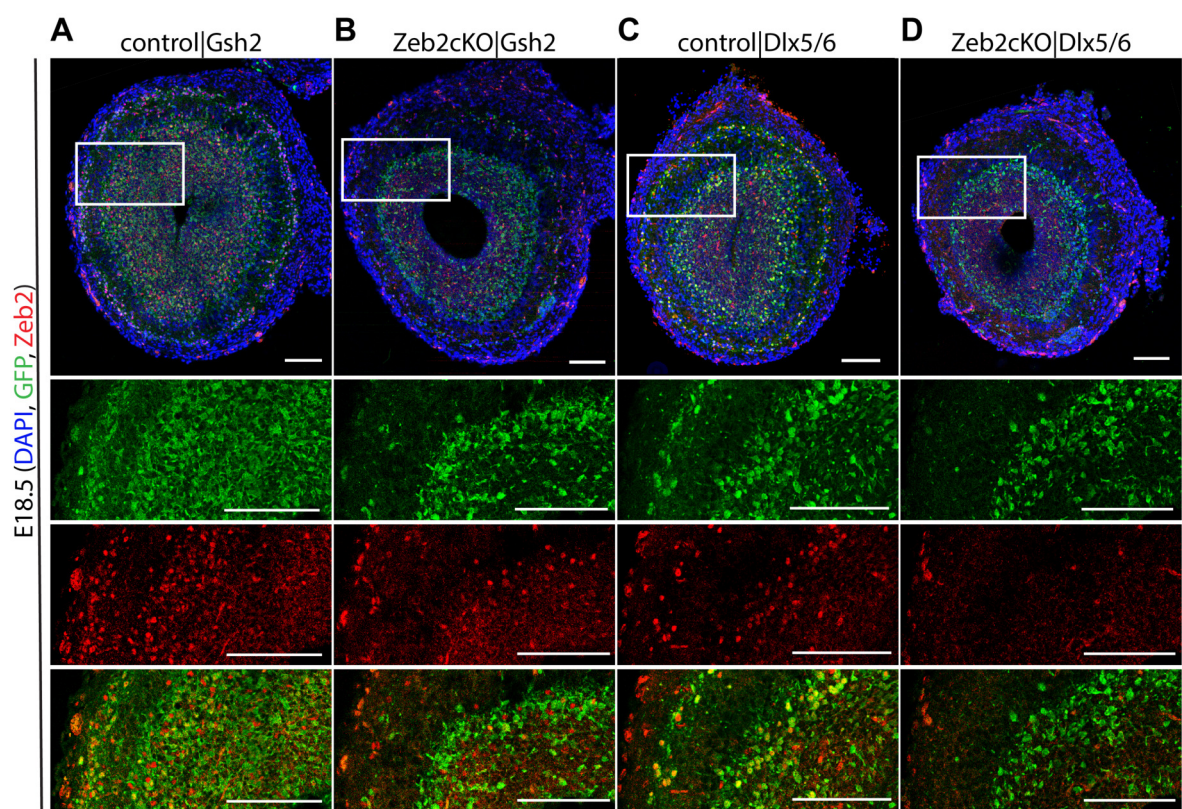


Figure S7. Proliferation is not significantly affected in *Zeb2*-cKO cells.

A. Schematic representation of a coronal section through the E18.5 telencephalon, depicting the V-SVZ in blue. The boxed area in panel A indicates the respective regions shown in panels B-C. **B-C.** Immunohistochemistry for GFP and PH3 in the E18.5 Gsh2 control and *Zeb2*-cKO V-SVZ showing no differences in number of proliferating cells compared to the control. Quantification in D (for GFP-: 211.8 in control vs 243.0 cells/mm² in cKO, p=0.4; for GFP+: 58.7 in control vs 58.11 cells/mm² in cKO, p=1, two-way ANOVA, n=3). **E.** At 18.5 in the Dlx5/6|*Zeb2*cKO and control V-SVZ, no significant differences in GFP+;PH3+ or GFP-;PH3+ were observed (for GFP-: 145.1 in control vs 147.2 cells/mm² in *Zeb2*-cKO, p=1; for GFP+: 20.81 in control vs 28.53 cells/mm² in *Zeb2*-cKO, p=0.94, two-way ANOVA, n=3).

F. Schematic representation of a coronal section through the P5 telencephalon, depicting the V-SVZ in blue. The boxed area in panel F indicates the regions shown in panels G-H. **G-H.**

Immunohistochemistry for GFP and Ki67 in the P5 Gsh2 control and *Zeb2*-cKO V-SVZ demonstrating a specific decrease of proliferating non-targeted (Ki67+;GFP-) cells in the *Zeb2*cKO|Gsh2 compared to the control. Quantification in I (for GFP-: 1867 in control vs 1048 cells/mm² in cKO, p<0.01; for GFP+: 1167 in control vs 1204 cells/mm² in cKO, p=0.97, two-way ANOVA, n=5).

J-L. Immunohistochemistry for GFP and Ki67 in the P5 V-SVZ after P2 electroporation of a Cre expression plasmid in control|WT (J) and *Zeb2*cKO|WT (K) mice. Quantification in L shows no significant difference in proliferating cells in the cKO compared to control (52.7 in control vs 60.3 GFP+;Ki67+/GFP+ cells, two-tailed t-test, p=0.16, n=3).

Error bars indicate SEM, scale bars always represent 100 μm. Abbreviations: CTX, cortex; LV, lateral ventricle; STR, striatum; V-SVZ, ventricular-subventricular zone.

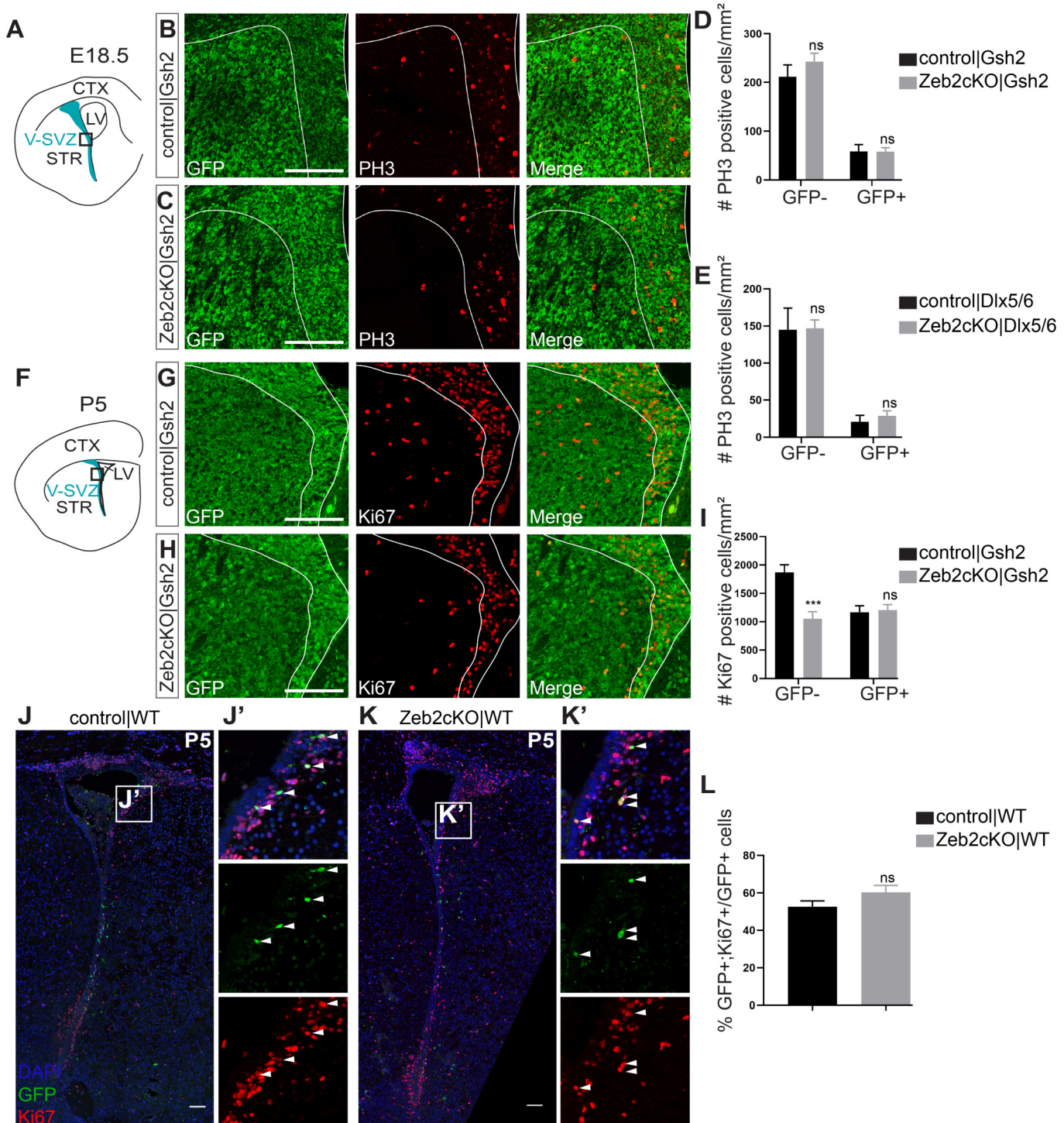


Figure S8. Zeb2 directly binds to promoter-proximal region of Sox6

Zeb2 binding to the *Sox6* promoter region, tested by ChIP using anti-Zeb2 antibody (ChIP) versus rabbit IgG (IgG) as negative control. Amylase represents the control for a non-Zeb2 binding gene. 5kb upstream the Transcription Start Site (TSS=0) have been scanned using Jasper Database for putative Zeb2-binding sites (Remacle *et al.*, 1999), and are here indicated as red lines. Regions indicated as E1 to E10 represent amplicons obtained by qPCR using the primers reported in Table S2. Zeb2 detectably bound to *Sox6* promoter E2-box-like sites at d6 and d8 of mouse ESC neural differentiation.

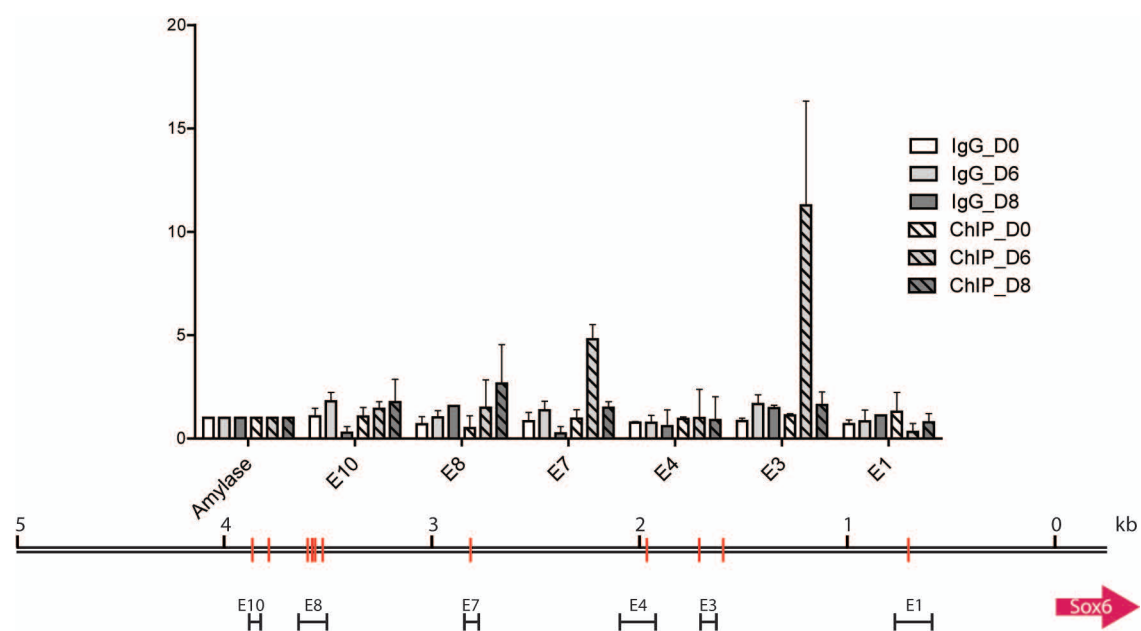


Table S1. qPCR primers

Primer	Forward	Reverse
Amylase	CTCCTTGTACGGGTTGGT	AATGATGTGCACAGCTGAA
Sox6_E1	CTGCCACTAATGAGAGAGAC	CATGTTGACTGAATGGCTTC
Sox6_E2	GCTTTAGGGAAAATGGATTG	GTGTAGTGGGTCTTCATTG
Sox6_E3	CATGTGTGCATGTATTCCTC	ATGTTCTAAAGAGCACCGTT
Sox6_E4	ACATTTGCGTTTGTGTCA	CGAATGAATGAGTTGACTGC
Sox6_E7	AACACAACAACCAAGCTACT	TCTCGCATCAAGGTATTCCTC
Sox6_E8	TTAGTTGTGTGGACATAGC	ACTACAACGGTGTCCATA
Sox6_E9	AGAGGTGGAGTGTATGGAAA	TCAACTTGGTGAAACCCTT
Sox6_E10	GCTTCCTAAAGTACAGCTCA	GAGACCAGAGGACAACATTG
Zeb2_KO	GAACTAGTTGAATTGGTAGAATCAATGGG	AAGCATGTCGGTAAGCTGACCAACTACTAG